

Report on laser-induced fluorescence transitions relevant for the microelectronics industry and sustainability applications

V. S. Santosh K. Kondeti,^{1, a)} Shurik Yatom,¹ Ivan Romadanov,¹ Yevgeny Raitses,¹ Leonid Dorf,² and Andrei Khomenko²

¹⁾*Princeton Plasma Physics Laboratory, Princeton, New Jersey.*

²⁾*Applied Materials, Santa Clara, California.*

(Dated: 13 June 2024)

A wide variety of feed gases are used to generate low-temperature plasmas for the microelectronics and the sustainability applications. These plasmas often have a complex combination of reactive and non-reactive species which may have spatial and temporal variations in the density, the temperature and the energy. Accurate knowledge of these parameters and their variations is critically important for understanding and advancing these applications through validated and predictive modeling and design of relevant devices. Laser-induced fluorescence (LIF) provides both spatial and temporally resolved information about the plasma-produced radicals, ions, and metastables. However, the use of this powerful diagnostic tool requires the knowledge of optical transitions including excitation and fluorescence wavelengths which may not be available or scattered through a huge literature domain. In this manuscript, we collected, analyzed and compiled the available transitions for laser-induced fluorescence for more than 160 chemical species relevant to the microelectronics industry and the sustainability applications. A list of species with overlapping LIF excitation and fluorescence wavelengths have been identified. This summary is intended to serve as a data reference for LIF transitions and should be updated in the future.

Keywords: Laser-induced fluorescence, etching, microelectronics, sustainability

^{a)}Electronic mail: vkondeti@pppl.gov

I. Introduction

According to the Moore's law, the number of transistors on a chip exponentially increase every year¹⁻⁴. The semiconductor industry has been able to keep up with this law by the use of the low-temperature plasma based processes to perform operations such as etching, deposition, or cleaning. The microelectronics industry widely uses plasma-based deposition techniques such as sputtering, plasma-enhanced chemical vapor deposition, oxidation, and planarization⁵. Film and material removal techniques such as etching, photo resist stripping, and cleaning⁵ also involve plasma-material interactions. The underlying material science and the plasma-surface interactions are not completely understood, which poses a significant challenge to develop new tools for the industry. The fabrication of microelectronics in the present era requires sub-nm precision accuracy to enable technologies such as the 3 nm and the 2 nm nodes⁶. Modern microelectronics industry uses processes such as atomic layer etching (ALE), atomic layer deposition (ALD), area selective deposition and high aspect ratio processing to achieve such precision⁷⁻¹². Achieving such precision without damage to the underlying material layer will require meticulous control over the ion energy (or velocity) distribution function (IEDF/IVDF), the fluxes of ions and radicals and the chemical composition near the material surface^{13,14}.

Since their inception, the standard diameter of the silicon wafers used in the microelectronics industry has been increasing to enhance the throughput and reduce the operational cost. Starting from a wafer diameter of 12.5 mm in the year 1957, the industry currently uses a size of 300 mm and proposes to use a size of 450 mm in the future¹⁵. This increase in wafer size necessitates larger plasma chambers. Radio-frequency capacitively coupled plasmas are known for generating large-scale self-organized patterns, leading to spatial non-uniformities that become particularly critical in larger chambers¹⁶. Etching and deposition occurs on the silicon wafer surface and it is essential to know the chemical and plasma properties close to the wafer surface. The control over the processes occurring on the wafer surface can be achieved by understanding the chemical stoichiometry close to the wafer surface¹⁷. The measurement of the spatial variation in the properties of the radicals, ions and metastable species will help in determining the operational parameters that generate a spatially uniform plasma.

Material processing is often controlled by using a pulsed plasma with a duty cycle that allows for periodic intervals where ions or radicals are acting on the material. The volatile products from the material surface are removed during the plasma-off phase. Ions are accelerated towards the material surface by applying a bias voltage on the material surface. By varying the duty cycle of the pulsed plasma, a reproducible high aspect ratio anisotropic etching can be achieved^{13,14}. The measurement of the temporal variation of the radicals, ions and metastable species in a pulsed plasma will validate the simulation models, that are widely used in the microelectronics industry.

The emergence of alternative materials with unique properties such as a single atomic layer or thin films, two-dimensional materials, materials with controlled defects, and nanocrystal assemblies, the semiconductor industry is entering a new post-silicon era¹⁸. These materials include group III, IV materials, MoS₂, WSe₂, graphene, TiO₂, VO₂, SmNiO₂ and others^{19,20}. The post-silicon era materials are of interest for quantum computing, quantum electronics, and quantum photonics²¹.

Similar to low-pressure plasmas used in the microelectronics industry, atmospheric pressure plasmas which are widely used for sustainability applications, can also involve a complex chemistry^{6,22,23}. These plasmas are used for a wide variety of existing and emerging applications such as plasma medicine²⁴, plasma agriculture²⁵, plasma synthesis of nanomaterials²⁶, plasma catalysis^{27,28}, thermal plasmas for welding, cutting and spraying²⁹, plasma-assisted combustion³⁰, environmental applications^{31,32}, pollution control^{33,34}, additive manufacturing³⁵ and others. These plasmas operate at atmospheric pressure (1 atm) and do not require vacuum hardware to generate the plasma. All these applications require the interaction of plasmas with solids and liquids^{36,37}.

While the plasmas used in the microelectronics industry can be tens of cms in dimensions, the plasmas used in sustainability applications vary in size from microplasmas (μm - mm size)³⁸ to large volume reactors (several cm's)³⁹. Microplasmas have large gradients in the density of ions, electrons and radical species over a dimension of a mm. Large-volume reactors can result in a spatially non-uniform discharge. To avoid forming filamentary discharges, the atmospheric pressure plasmas are often generated using pulsed voltage waveforms with a duty cycle. So, the plasma is on only for a fraction of the time. Similar to the use of pulsed plasmas for processing of microelectronics, it results in an intermittent plasma with a temporal variation of

the density of electrons, ions, and radicals generated by the plasma.

The predictive design capabilities of the plasma sources used for the microelectronics and the sustainability applications can be developed by the comprehensive modeling of the plasma reactors involving hybrid fluid simulations. Modeling is often plagued by the lack of the chemical kinetics information and the experimental data to validate the simulation results. Measurement of the spatial and temporal variation in the IEDF/IVDF, ion/radical/metastable density distributions and gas temperatures can inform and improve the predictive capabilities of the simulations. Non-intrusive optical diagnostic techniques such as optical emission spectroscopy and absorption spectroscopy are line-of-sight integrated techniques and obtaining spatially resolved information requires the assumption of a spatial profile.

A laser-based technique such as laser-induced fluorescence can resolve both the spatial and the temporal information, while being non-intrusive. Being a resonant laser-based technique, it can detect species even if there is no detectable optical emission from the plasma, in addition to when there is optical emission from the plasma. The LIF transitions for various species such as ions, atoms and molecules is spread over different scientific papers from various fields. It is often not straightforward to find the different species that can be detected by LIF and the various reported transitions previously reported for a particular species. In this work, we reviewed the basic principles of LIF and the different types of LIF applicable for the microelectronics industry and the sustainability applications. We compiled a LIF reference database with the available LIF transitions that will enable the measurement and the detection of the various plasma-produced ions, radicals, and metastables that are relevant for microelectronics and sustainability applications. We describe the principle, the required instrumentation, calibration and the applications of LIF in section II. Section III provides the compilation of the LIF transitions and we summarize in section IV.

II. Laser induced fluorescence

A. Introduction and principle

Laser-induced fluorescence can provide both spatial and temporal measurements of the plasma-produced neutral, ionic, and metastable species. In LIF, laser irradiation resonantly excites the plasma-generated

species to a higher electronic state. The excited species emit fluorescence upon relaxation to a lower level. This fluorescence intensity can be used to quantify the species density and the velocity distribution functions^{40–48}. When the wavelength required for a resonant transition in LIF falls in the vacuum ultraviolet (VUV) region that is readily absorbed by the ambient air and water vapor, a two-photon excitation scheme is used and the technique is called two-photon absorption laser-induced fluorescence (TALIF). In this method, the energy required for exciting to the upper level is provided by two photons. A schematic of the excitation schemes for LIF and TALIF is shown in Figure ??(a).

LIF has been used for measuring relative/absolute densities of neutral radical species⁴¹, velocity distribution functions (VDF)⁴⁹ and rotational temperatures of molecules⁵⁰. Densities as low as 10^8 cm^{-3} have been successfully measured by LIF when using sensitive modern optical sensors such as a photomultiplier tube (PMT) or an intensified charge-coupled device (iCCD) camera⁵¹. The spatial resolution of LIF is about 100–200 μm . Absolute densities of neutral radicals can be obtained through calibration of the fluorescence signal. Rayleigh scattering from a known concentration of air coupled with a multi-level model is typically used for obtaining absolute densities for one-photon LIF schemes. Fluorescence from the two-photon excitation of a known concentration of a neutral gas is used for the calibration of TALIF schemes. Details of the calibration methods have been summarized in section II C. For obtaining absolute densities, the laser energy in the LIF measurements is maintained in the linear regime, i.e., when the LIF intensity is proportional to the laser energy. This ensures that the ground state density does not get depleted by the laser beam and the laser energy is spent in the excitation from the lower level to the higher level rather than from the stimulated emission from the higher level to the lower level. Fully saturated laser induced fluorescence has also been used for detecting species using LIF. In the fully saturated LIF regime, a high laser energy is used that ensures that the stimulated emission dominates over the spontaneous emission and the collisional quenching of the excited state^{52,53}. Further, saturation will broaden the LIF absorption line profiles and modify the line profile to a Lorentzian shape^{54,55}. Saturation broadening needs to be accounted for deducing the velocity distribution function. While fully saturated LIF has been used to get a better signal to noise ratio, it is difficult to determine the fully saturated regime and maintain such saturation over the entire interrogation volume^{52,53}. For TALIF measurements, the used laser energy is in the quadratic regime where the TALIF

intensity is proportional to the square of the laser energy to avoid the consequences of saturation effects described above. LIF signal intensities can be reduced due to quenching of the excited state by the feed gases, humidity, air, and molecular gases such as the ones used in the microelectronics industry. A correction of the fluorescence intensity due to the presence of such quenchers needs to be accounted to obtain absolute densities⁵⁶⁻⁵⁸. Resonant transitions from the ground state are often not available for all atomic and molecular species. Excitation from the metastable states of neutrals and ions has been used as a proxy for ground state species by assuming thermal equilibrium between the metastable and the ground states. This allows to obtain useful information about the species velocities that are important for applications with plasma flows such as ion sources and plasma thrusters^{55,59-61}. The metastables in a plasma are predominantly produced by the presence of electrons with the appropriate energy. The absence of electrons with such energy, quenching due to collisions or ionization can deplete or reduce the density of density of the metastable states below the detection limit of LIF. Hence, the application of LIF for metastable excitation may not be applicable to a wide variety of discharge environments.

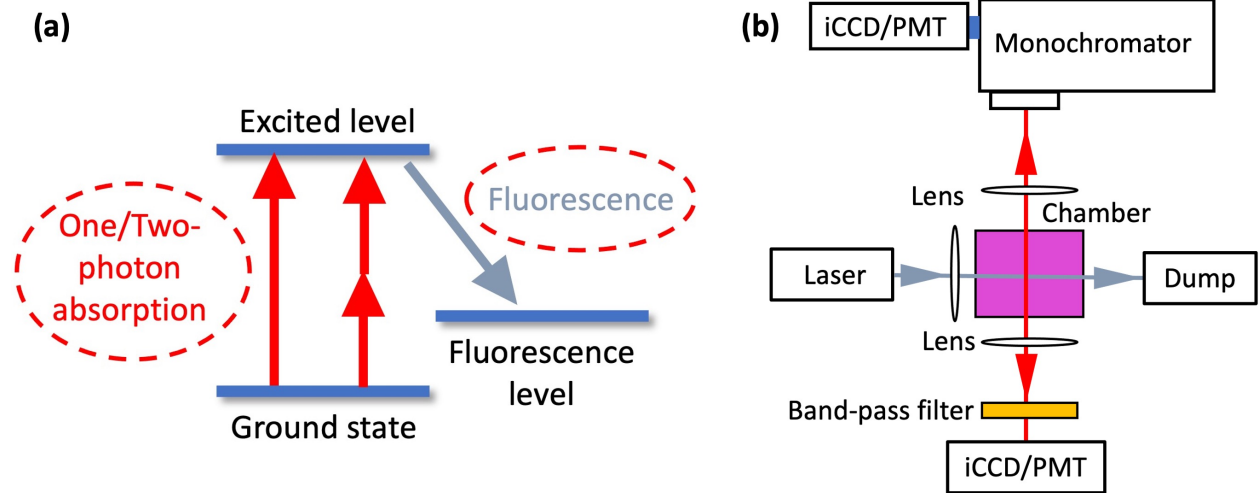


FIG. 1: (a) Transitions schematic and (b) Experimental schematic of laser-induced fluorescence

B. Implementation and instrumentation

The laser beam is focused on to the plasma and the fluorescence is typically detected perpendicular to the laser beam propagation by a detector (Figure ??(b)). The spatial resolution in LIF is limited by the

focus size of the laser launch and the collection optics. The laser beam is imaged onto the detector by using a lens. Using a PMT results in a point measurement and the spatial distribution can be obtained by using diaphragms and positioning the PMT to image different regions of the laser beam. The wavelength of fluorescence is typically different from the laser excitation wavelength. However, the fluorescence detection at the same wavelength as the excitation wavelength has also been reported⁴⁵. In such situations, fluorescence is detected with a certain delay after the laser beam. This technique relies on the longer lifetime of the laser excited level than the pulse width of the laser beam. When the laser excitation wavelength is different from the fluorescence wavelength, an appropriate narrow band-pass filter or a cut-off filter is installed in front of the detector to transmit only the fluorescence onto the detector or block the Rayleigh scattering of the laser beam. When a fluorescence spectrum is desired, the laser beam is imaged onto the entrance slit of a monochromator that is coupled with an iCCD camera or a PMT. The shaping of the laser beam into a sheet provides a two-dimensional distribution of the imaging species and this technique is called planar laser-induced fluorescence (PLIF)⁶²⁻⁶⁵. PLIF can provide the spatial distribution of non-uniformities in the discharge with a single measurement (Figure ??(b)). Examples of the measured OH density using LIF and PLIF are shown in Figure 2(a) and 2(b). For obtaining time-resolved information on the plasma-produced species in a pulsed plasma, a pulsed laser is typically used. The temporal resolution is limited by the pulse width of the laser beam. An example of the time resolved OH density measured in a pulsed plasma is shown in Figure 2(a). Nanosecond pulsed laser beams are a popular and a cost-effective way for executing LIF, while the relatively more expensive picosecond and femtosecond lasers have also been used for performing LIF⁶⁶⁻⁶⁸.

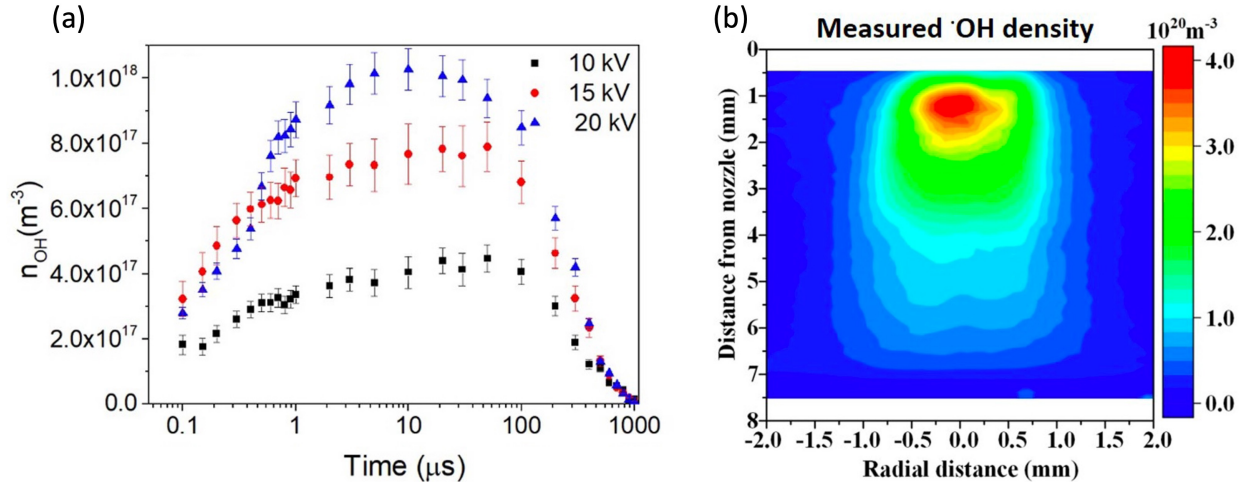


FIG. 2: Examples of absolute OH density measured using (a) LIF of a pulsed dielectric barrier discharge⁶⁹ and (b) PLIF of an RF plasma jet (reproduced from Ref.⁵⁶ with permission from the American Vacuum Society (AVS)).

Depending on the application, different types of lasers have been used to perform LIF measurements. These include solid state lasers, dye lasers, diode lasers, quantum cascade lasers and optical paramagnetic oscillators (OPO)^{70,71}. Diode lasers can have a line-width down to the fm range, while dye lasers typically have line-widths in the pm range and commercial OPO lasers have line-widths in the range of tens to hundreds of pm. The narrow line-width of diode lasers allows the accurate resolution of the narrow spectral features of atomic, ionic and molecular transitions. These lasers can be applied to detect precise Doppler shifts in the transition. These shifts can be caused by velocity changes as small as tens of m/s along the direction of the laser beam propagation (Section II E). The inherent large line-width of the dye lasers and the OPO lasers compared to the diode lasers limits their application to measuring only large Doppler shifts that are produced by very high ion or atom velocities⁷². The dye lasers and the OPO lasers offer the ability to generate a broad range of wavelengths ranging from the deep ultraviolet (DUV) to the infrared region. Solid state lasers, diode lasers and quantum cascade lasers often generate radiation only in a narrow spectral region and do not have the versatility to generate a broad range of wavelengths.

C. Calibration method for obtaining absolute density for LIF

The LIF signal can be calibrated to obtain absolute densities of the ground state species. The LIF signal can be described by the following equation^{51,73}:

$$I_{LIF} = \frac{1}{4\pi} \int (\eta_{LIF} \frac{hc}{\lambda_{fl}}) n_{exc}(x, y, z, t) A_{fl} dx dy dz dt \quad (1)$$

Where η_{LIF} is the instrumental factor that is the product of quantum efficiency of detector, transmission of the optical setup and the solid angle of signal collection, h is the Planck's constant, c is the speed of light, $n_{exc}(x,y,z,t)(m^{-3})$ is the density of the excited level, from which the fluorescent photons are emitted, λ_{fl} is the fluorescence wavelength (m), A_{fl} - Einstein coefficient of the fluorescent transition (s^{-1}). The unknown parameters in this equation are η_{LIF} and n_{exc} . This section describes a method to calculate the ground state density n by using Rayleigh scattering and a population kinetics model.

1. Rayleigh scattering

The experimental setup for implementing this calibration method is similar to the experimental setup used for executing LIF (Figure ?? (b)). The plasma is turned off and the region of interest is filled with a gas such as air. The spectral filter that was used for LIF is removed and the laser beam is imaged on to the detector to collect the Rayleigh scattering signal from air. If a monochromator was used for LIF, the wavelength window of the monochromator is adjusted to detect the Rayleigh scattering laser beam. The position of the detector is not changed compared to the LIF setup to ensure that the solid angle of detection is the same as that for the LIF measurements.

The Rayleigh scattering signal (I_R) can be described as^{51,73,74}:

$$I_R = \eta_R N_n \left(\frac{\partial \sigma_0}{\partial \Omega} \right) E_L \Delta x \quad (2)$$

Where N_n is the scattering particles density, E_L is the laser pulse energy, Δx is the the detection volume

length, η_R is the instrumental factor for the wavelength of the Rayleigh scattering, and $\frac{\partial\sigma_0}{\partial\Omega}$ is the Rayleigh scattering differential cross-section. The differential Rayleigh scattering cross-section depends on the polarization direction of the laser beam and the angle at which the scattering light is collected. A convenient configuration is when the polarization of the laser beam is perpendicular to the laser propagation direction and the Rayleigh scattering collection is at angle of 90° with respect to the laser propagation direction and the polarization direction. Assuming that the detector collects all polarizations of the scattered beam, the differential Rayleigh scattering cross-section is defined as⁷⁴:

$$\frac{\partial\sigma_0}{\partial\Omega} = \frac{3\sigma}{8\pi} \frac{2}{(2 + \rho_0)} \quad (3)$$

Where σ is the total Rayleigh scattering cross-section (m^2), ρ_0 is the ratio of the horizontally-to-vertically polarized light in an unpolarized laser beam. The subscript 0 corresponds to the detection of both horizontal and vertical polarization of the scattering. The values of σ , ρ_0 for the commonly used scattering from air are tabulated as functions of wavelength in the review by R. Miles *et al.*⁷⁴. Calibration using Rayleigh scattering is usually performed at a known pressure and temperature. The scattering particles density can be obtained by using the ideal gas law⁷⁵:

$$N_n = \frac{P}{k_B T} \quad (4)$$

Where k_B is the Boltzmann constant. To calculate the instrumental factor, η_R in equation 2, the Rayleigh scattering intensity is measured for several laser energies at a fixed pressure. The slope of the straight line curve (α) is calculated by plotting the Rayleigh scattering intensity (I_R) as a function of the product of the laser pulse energy, E_L and the pressure, P (Figure 3).

$$\alpha = \frac{I_R}{PE_L} = \frac{\eta_R \Delta x}{k_B T} \left(\frac{\partial\sigma_0}{\partial\Omega} \right) \quad (5)$$

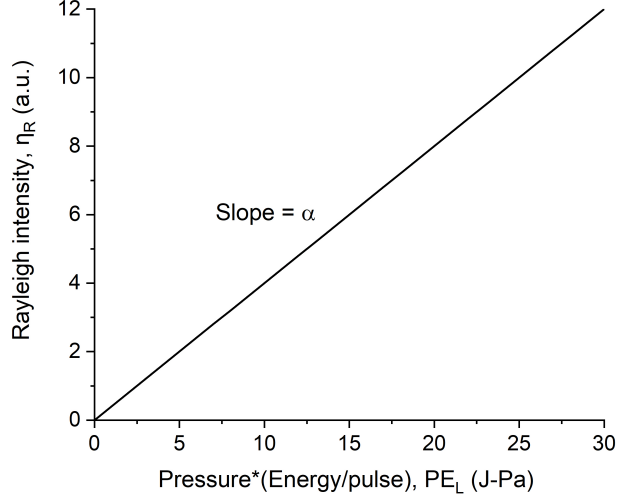


FIG. 3: An example to determine the instrumental factor by Rayleigh scattering.

The instrumental factor reduces to:

$$\eta_R = \frac{\alpha k_B T}{\left(\frac{\partial \sigma_0}{\partial \Omega}\right) \Delta x} \quad (6)$$

The wavelength of the LIF signal is different from the laser excitation wavelength. The instrumental factor depends on the efficiency of the detector at the wavelength of detection. Hence, the instrumental factor for LIF needs to be corrected for the detector efficiency at the two different wavelengths. So, $\eta_{LIF} = \eta_R \frac{\epsilon_{LIF}}{\epsilon_R}$, where ϵ_{LIF} and ϵ_R are the products of the transmission factor of the optics and the quantum efficiency of the detector at the LIF and Rayleigh scattering wavelengths respectively. This correction can be avoided by setting the laser wavelength to the LIF wavelength for Rayleigh scattering measurements. However, a large difference between the LIF wavelength and the laser excitation wavelength for such a measurement might shift the laser beam path, the energy density of the focused laser beam can be different and such large wavelength shift may not be in the tunable range of the laser being used.

2. Laser parameters and population kinetics model

Several parameters are required to develop for the population kinetics model and we define them here. The time evolution of the laser irradiance ($I_L(t)$) is defined as^{51,73}:

$$I_L(t) = \frac{E_L \Gamma^{<1>}}{\Delta\nu_L \tau_L A_L} L(t) \quad (7)$$

Where $\Gamma^{<1>}$ is the dimensionless one-photon overlap integral, $\Delta\nu_L$ is the laser line-width (m^{-1}), A_L is the area of the laser beam at the detection location (m^2) and $L(t)$ is a normalized function that describes the temporal evolution of the laser pulse. $\Delta\nu_L$ can be obtained from the specifications sheet of the laser. A_L can be measured by a laser camera. Assuming the beam profile of the laser beam, it can also be calculated by measuring the residual laser energy by traversing a knife edge at the measurement location. I_L can be measured by measuring the Rayleigh scattering intensity with a short gate time at different delay times with respect to the laser beam. The dimensionless one-photon overlap integral is defined as⁷⁶:

$$\Gamma^{<1>} = \Delta\nu_L \int_{-\infty}^{+\infty} P_{abs}(\nu) P_L(\nu) d\nu \quad (8)$$

Where P_{abs} is the absorption transition spectral profile (m) and $P_L(\nu)$ is the laser spectral profile (m). P_{abs} can be calculated by measuring the absorption profile and accounting for the different broadenings such as Van der Waals broadening and Doppler broadening^{51,69,73}. $P_L(\nu)$ can be taken from documentation of the laser manufacturer.

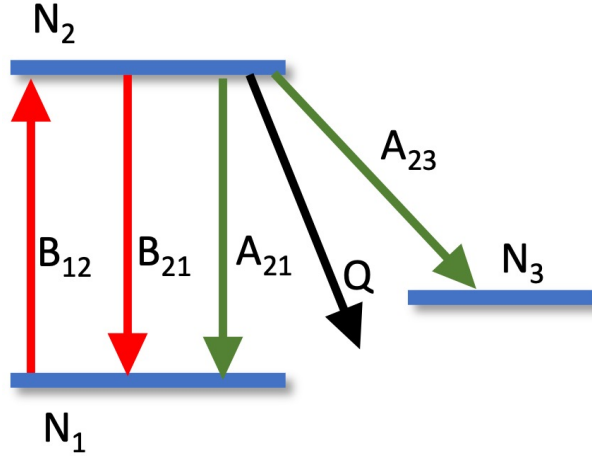


FIG. 4: A three-level model of LIF. A_{ij} : spontaneous optical transitions, B_{ij} : Laser-induced transitions, Q : Collision induced transitions.

The LIF signal is related to the population density of the excited state species n_{exc} (equation 1). A population kinetics model is used to deduce the ground state density. We illustrate a 3-level model here (Figure 4). A 4, 5 and 6-level model has also been implemented^{41,51,73,77,78}. Upon laser irradiation, several processes occur that result in the measured LIF signal. These include laser excitation from the ground state to the excited state, laser de-excitation from the excited state to the ground state, spontaneous relaxation from the excited state to any lower energy level and collisional quenching of the excited state. While there can be an additional source of production that can increase the density of these different levels, it is often neglected in the analysis. This is done by assuming the level to be in a quasi-steady state, where the laser excitation and its subsequent de-excitation is the most dominant process that results in the changes of the population of these states. A set of time dependent differential equations are solved to obtain the ground state density^{41,51,73,77,78}.

The time dependent differential equations for a 3-level model are described below.

$$\frac{dN_1}{dt} = I_L(t)(B_{21}N_2f_B^2 - B_{12}N_1f_B^1) + A_{21}N_2 \quad (9)$$

$$\frac{dN_2}{dt} = I_L(t)(B_{12}N_1f_B^1 - B_{21}N_2f_B^2) - QN_2 \quad (10)$$

$$\frac{dN_3}{dt} = A_{23}N_3 \quad (11)$$

Where N_i is the density of the level i normalized to the ground state species density n , $I_L(t)$ is as defined in equation 7, B_{ij} is the Einstein B coefficient from level i to level j (mJ^{-1}), A_{ij} is the Einstein A coefficient from level i to level j (m^3s^{-1}), f_B^i is the temperature-dependent Boltzmann factor of the level i and Q is the quenching rate of the excited level. The Einstein A coefficient, the Einstein B coefficient and the Boltzmann factor are available from literature for several species⁷⁹. This information is not readily available for all the species of interest. The Einstein A coefficient for atomic species is available from the NIST database⁷⁹, while it is available for several molecular species in the cited references in the tables⁸⁰. The Einstein B coefficients are available for well studied species in the references provided in the tables. The Boltzmann factor needs to be calculated for the specific energy levels involved in the transitions^{81,82}. For the ground state and the metastable level atomic species, the Boltzmann factor can be assumed to be unity. However, for resonant atomic levels, the population of the resonant levels need not be larger than the other resonant levels involved in the transitions. For example, LIF can be performed by exciting the $\text{Ar}(1s_2)$ and the $\text{Ar}(1s_4)$ resonant levels, which are the ground states for excitation of these species. The validity of f_B being taken as unity needs to be carefully examined for each case. Q can be estimated by measuring the fluorescence decay time constant after accounting for the collisions with different species⁵¹. These equations are solved to obtain the ground state density of the species.

D. Calibration using a known concentration of a gas for TALIF

TALIF is a non-linear two-photon excitation process⁶⁶. This does not allow the use of Rayleigh scattering to calibrate the fluorescence intensity to deduce the absolute density of the species discussed in section II C 1. The experimental setup for TALIF calibration is the same as the setup used for collecting the TALIF signal (Figure ??(b)). In this method, a known concentration of a reference gas is excited to a higher level using two-photon excitation by a laser. The reference gas is chosen such that the two-photon excitation wavelength of the reference gas is spectrally similar to the excitation wavelength of the species whose absolute density needs to be determined. The position of the detector for the TALIF of the measured species and the reference gas setup is the same. The TALIF signal from the reference gas can be collected by using an appropriate spectral filter or by setting a monochromator to transmit the desired wavelength. The used laser energy is in the quadratic regime for both the reference gas and the detection species to avoid correction for the complicated saturation effects. The TALIF signal (I_{TALIF}) can be defined as^{56,57,66}:

$$I_{TALIF} = T \frac{\sigma^{(2)} a \Gamma^{<2>} n}{(h\nu)^2} \quad (12)$$

Where T is the instrumental factor, $\sigma^{(2)}$ is the two-photon absorption cross-section, $h\nu$ is the photon energy, $\Gamma^{<2>}$ is the dimensionless two-photon overlap integral between the laser spectral profile and the two-photon absorption profile⁷⁶ and n is the species density. $\sigma^{(2)}$ is available for different species in the cited references of the tables. The branching ratio (a) is defined as^{57,66}:

$$a_i = \frac{A_{ik}}{A_i + \sum_q k_q n_q} \quad (13)$$

where the subscript q refers to the quenching species, A_{ik} is the spontaneous emission coefficient of the observed fluorescence line from level i to level k , A_i is the total spontaneous emission rate from the excited level i , k_q is the quenching coefficient and n_q is the density of the quenching species assuming that the 3-body

collisional quenching is negligible⁸³.

The dimensionless two-photon overlap integral is the two-photon analogue to the one-photon overlap integral defined in equation 8. It is defined as⁷⁶:

$$\Gamma^{<2>} = \Delta\nu_L \int_{-\infty}^{+\infty} \int_{-\infty}^{+\infty} P_{abs}(2\nu)P_L(\nu)P_L(\nu)d\nu d\nu \quad (14)$$

The TALIF signal from both the reference gas (I_r) and main species (I_m) are collected. The density of the main species reduces to⁶⁶:

$$n_m = \frac{T_r \sigma_r^{(2)} a_r}{T_r \sigma_m^{(2)} a_m} \left(\frac{h\nu_m}{h\nu_r} \right)^2 \frac{I_m \Gamma_r^{<2>}}{I_r \Gamma_m^{<2>}} n_r \quad (15)$$

where the subscripts m and r refer to the main species and the reference gas respectively^{66,83}.

E. Laser-induced fluorescence for velocity distribution functions

LIF is a crucial optical measurement technique for characterizing the flows and studying the kinetic processes in plasmas^{55,84,85}. LIF allows for measurements of the VDF, which is essential for understanding the thermodynamic state of a medium. This function allows us to derive important parameters such as the temperature, the mean velocity, and the most probable velocity from the fluorescence profile. Moreover, LIF can directly measure the electric and the magnetic fields in plasmas through the Stark⁸⁶ and the Zeeman effects⁸⁷ respectively. It is also possible to indirectly determine the electric fields by analyzing the moments of the VDFs⁸⁸. LIF utilizes the Doppler effect, where the absorption of the light occurs at a frequency shifted from the resonant transition frequency, a shift that depends on the velocity of the moving atom or the ion. Thus, it is sometimes referred to as Doppler-shift LIF.

The LIF process consists of two steps, as illustrated in Figure ??(a). In the first step, the species in the plasma are often in the excited state due to collisions with energetic electrons or other species. These states,

known as metastable states, have long lifetimes — up to seconds, compared to the fluorescence states. It is important to note that when a metastable state is excited to deduce the properties of the ground state species, an assumption about the thermal equilibrium between this state and the ground or other states of the probed species in the plasma is necessary. When a laser beam is introduced, these excited atoms or ions absorb photons and are further excited to a higher energy state. The selection of this transition is guided by rules based on various quantum numbers⁸⁹ and must be sufficiently populated to ensure a detectable signal⁹⁰. Plasma parameters, such as the electron temperature and the electron density, influence the excitation rate and the de-excitation mechanisms such as quenching (e.g. collisions). To facilitate further excitation to a higher state, the photon energy (wavelength) of the laser must correspond precisely with the energy required for a resonant transition. However, due to thermal or directional motion of the probed species in the plasma, they perceive the incoming laser light wavelength Doppler-shifted (see Figure 5). This requires tuning of the laser wavelength to the target species moving at specific velocities.

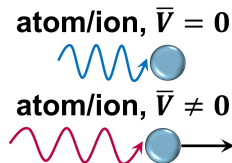


FIG. 5: A schematic of the Doppler effect.

In the second step of the process, the excited species emit light through spontaneous emission, collisions, or stimulated emission, transitioning to a lower energy state. This transition can be resonant, in case if the species return to their initial energy state, and non-resonant if decay leads to a different level. Non-resonant emission is typically utilized in Doppler-shift LIF diagnostics because it allows the emitted wavelength to be easily distinguished from the intense laser light. The intensity of the emitted light is directly proportional to the number of species moving at the targeted velocity. By measuring emissions at various excitation frequencies, one can reconstruct the VDF, yielding detailed parameters of the ions or the neutrals. A schematic of this process is shown in Figure 6(a). When the laser frequency is scanned across the Doppler broadened absorption profile, the excited species then emit the fluorescence light. This signal is detected by various methods described in section II E 3, and the profile of the VDF can be reconstructed (Fig. 6(b)).

Doppler-shift LIF can be characterized with a high spatial resolution of 100's of μm^{91} , a temporal resolution of 10's of μs^{92-94} , and a spectral resolution which in terms of velocity translates to as low a few m/s^{95} .

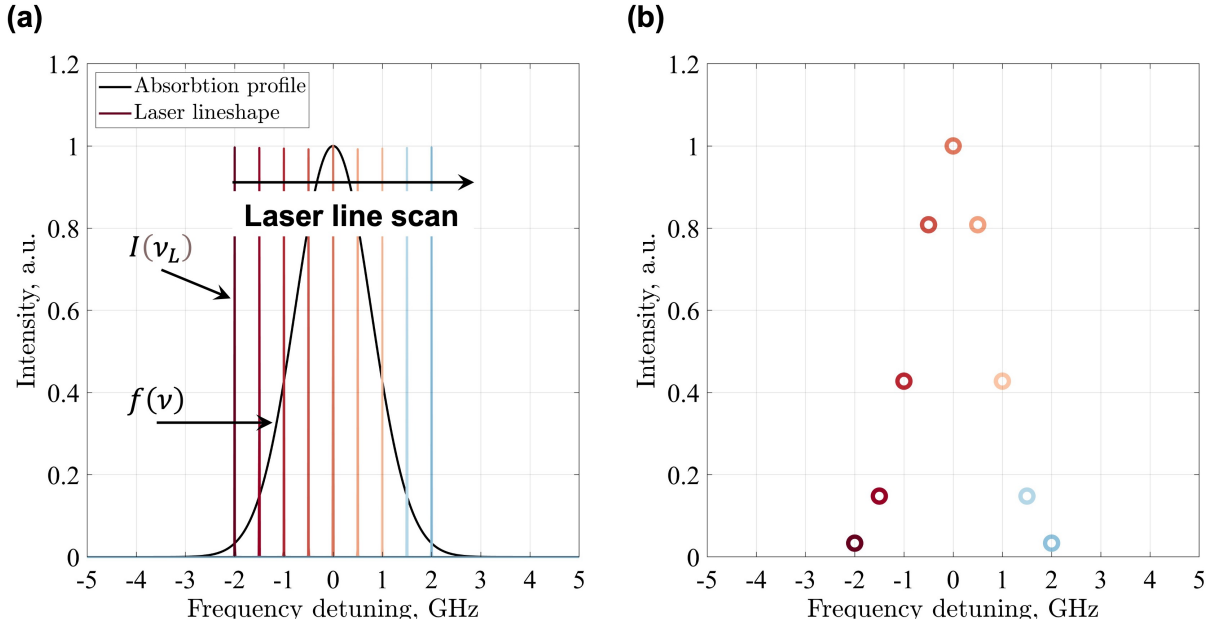


FIG. 6: Schematic of LIF measurements. a) Laser wavelength ($I(\nu_L)$) is scanned across the Doppler broadened absorption profile ($f(\nu)$). b) The recovered signal, which is proportional to the integral: $\int f(\nu)I(\nu_L)d\nu$. ν_L : laser wavelength.

1. Line shape

While Doppler broadening is the primary effect that allows us to extract information about the shape of the VDF, it is crucial to consider other mechanisms that might affect the measured line shape profile. In this subsection, we will discuss several physical mechanisms that contribute to the broadening of the line shape. Typically, the profile is influenced by broadening mechanisms such as hyperfine structure, isotopic splitting, Zeeman splitting, lifetime broadening, or Stark broadening. It is crucial to note that VDF measurements are feasible only under conditions where pressure broadening is not significant compared to the measured line-width of the LIF transition. This depends on the transition being probed and the operating conditions, for example at a pressure < 10 Torr⁹⁶. The measured LIF profile, denoted as $f_{LIF}(\nu_L)$, results from the convolution of the Doppler line shape with the effects of broadening mechanisms and the laser intensity. This relationship can be represented mathematically as follows:

$$f_{LIF}(\nu_L) \propto f(\nu_L) \otimes \phi_L(\nu_L) \otimes \phi_b(\nu_L) \quad (16)$$

where $f(\nu_L)$ represents the amplitude of the Doppler line shape, $\phi_L(\nu_L)$ is the laser intensity profile (typically negligible), and $\phi_b(\nu_L)$ includes all broadening mechanisms and is referred to as the Doppler-free line shape.

Doppler broadening arises from the thermal and the directional velocities of the species being probed. Consider a laser with a frequency of ν_L and a wave-vector of \mathbf{k} . For a moving particle with velocity \mathbf{v} , the shift in the laser frequency, $\Delta\nu$ in the specie's frame is given by:

$$\frac{\Delta\nu}{\nu_L} = -\frac{\mathbf{v} \cdot \mathbf{k}}{c} \quad (17)$$

where c is the speed of light. The transition frequency ν_T , at which the particle absorbs the laser, then becomes:

$$\nu_T = \nu_L + \Delta\omega = \omega_L \left(1 - \frac{v_k}{c}\right) \quad (18)$$

where (v_k) is the velocity component along \mathbf{k} . This establishes a direct correlation between the laser frequency and the particle velocities, facilitating the measurement of the VDF. LIF diagnostics involve scanning laser frequencies near the target transition and recording the fluorescence. Each frequency corresponds to a velocity group (v_k) of the species, allowing the velocity distribution to be mapped as a function of the laser frequency:

$$f_{LIF}(v_k) \sim F\left(\frac{\nu_T}{1 - \frac{v_k}{c}}\right) \quad (19)$$

This approach provides a one-dimensional representation of the VDF along the laser beam direction.

The broadening of the line shape due to the hyperfine structure of the energy levels and the isotope splitting significantly impacts the spectral profile. The hyperfine energy levels are determined by the total angular momentum \mathbf{F} , which results from the coupling between the total electron angular momentum \mathbf{J} and the nuclear spin \mathbf{I} , represented as $\mathbf{F} = \mathbf{J} + \mathbf{I}$. For example, among the nine isotopes of xenon, seven have zero nuclear spin due to an even number of neutrons and thus do not contribute to hyperfine structures, leaving only two isotopes that affect the line shape. This complexity in the hyperfine structure⁹⁷, can complicate the spectral analysis, especially since not all transitions have well-documented hyperfine structures. However, the most probable velocities can be discerned from the location of the LIF signal peak, which remains unaffected by this broadening mechanism. This allows for the characterization of flows and their variations. However, for more comprehensive analysis it is important to know the hyperfine structure and the isotope splitting of the species.

The lifetime broadening mechanism is related to the Heisenberg uncertainty principle, which posits that certain pairs of physical properties, like position and momentum or energy (E) and time (t), cannot be precisely measured simultaneously. This principle is mathematically expressed as:

$$\Delta E \Delta t \geq \hbar. \quad (20)$$

The uncertainty in the photon energy, $\Delta\omega$, is influenced by the lifetime of the upper energy level, τ_p . This relationship modifies the line shape into a Lorentzian function, as outlined in the literature⁹⁸:

$$\phi(\nu) = \frac{\Delta\nu}{(\nu - \nu_0)^2 + (\Delta\nu/2)^2}, \Delta\nu = \frac{1}{\tau_p}. \quad (21)$$

For instance, for the metastable level $5d^2[4]_{7/2}$ of Xe II, the lifetime ranges from 7 to 9 ns. The resultant broadening is significantly smaller by one or two orders of magnitude than that caused by the Doppler broadening, and thus can generally be neglected in analysis.

Two other mechanisms responsible for spectral line splitting are the Stark and the Zeeman effects. The Stark effect involves the line splitting due to the strong electric fields, which can induce additional angular momentum between the nucleus and the electron cloud. However, the electric fields must be considerably

strong to have a measurable impact. For instance, it was demonstrated that the Stark effect is negligible under typical plasma experimental conditions due to the field strengths involved⁹⁹. On the other hand, the Zeeman effect, which results from the influence of the magnetic fields, is more significant and can substantially alter the LIF line shape⁹⁶. This effect allows for the simulation of the spectral line splitting and the deduction of local magnetic field values, providing valuable insights into the magnetic environment within the plasma.

2. Laser systems

A tunable laser is essential for scanning the absorption profile in LIF experiments. It is important to distinguish between the continuous and the pulsed modes of the laser operation^{70,71}. Continuous wave (CW) lasers, such as laser diodes, have extremely narrow bandwidths, typically in the femtometer range or below. They allow for the direct observation of the species VDF in LIF measurements. Pulsed lasers, in contrast are broader in their line-width and deliver a large amount of energy per pulse, with pulse widths as short as a few femtoseconds, making them more suitable for time-resolved measurements.

The measurable VDFs vary with the type of the laser: diode lasers measure in the range of tens of m/s, while dye lasers and optical parametric oscillators (OPO) can detect velocities up to a few km/s and tens of km/s, respectively. As an example, the dependence of the laser line-width ($\Delta\lambda$) in *pm* on the ion velocity for argon and xenon ions has been shown in Fig. 7. Diode lasers are particularly effective for measuring the profiles of the velocity distributions, whereas dye and OPO lasers are better suited for detecting velocity drifts in systems with high-energy flows. However, it is important to note that in the case of high-resolution measurements, the limiting factor is usually a resolution of measurement system that detects the current laser wavelength, e.g. a wavemeter.

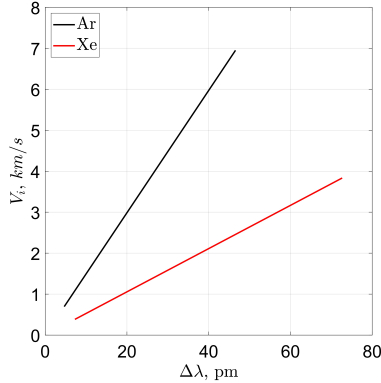


FIG. 7: The detectable argon and xenon ion velocities V_i as a function of the laser line-width, $\Delta\lambda$. The wavelength considered for the excitation of the Ar and Xe ions are 667 nm and 834 nm respectively.

CW diode lasers are commonly used in Doppler-shift based LIF, especially for noble gases. They offer wide tunability (up to 10 nm, depending on the design) and very narrow line-width. Additionally, they facilitate various high-frequency laser light modulations, such as amplitude and wavelength (or frequency) modulation, which are crucial for implementing detection methods based on homodyne¹⁰⁰, heterodyne⁴⁹, or photon counting principles^{101,102}.

3. Optical setup

The typical optical setup for the Doppler LIF measurements can be divided into two main components: the laser launch branch and the detection branch, as illustrated in Figure 8(a) and 8(b). The laser launch branch consists of optical elements tasked with the beam conditioning, directing, light modulation, and the measurement of the laser power and the laser wavelength. The beam conditioning involves a series of mirrors and lenses that direct and focuses the laser beam into the interrogation volume. Optical fibers may also be used to transport the laser beam. In some setups, the laser beam is shaped into a laser sheet for planar LIF measurements¹⁰³. The laser wavelength is controlled using a calibrated wavemeter. Additionally, a Fabry-Perot interferometer can be employed to monitor the quality of the laser mode in real-time and to detect any mode hops. The power of the beam is typically monitored continuously with a photodiode. The modulation of the laser wavelength or amplitude is an essential aspect of the setup. Amplitude modulation can be achieved using mechanical choppers, acousto-optic modulators (AOM), or electro-optic modulators

(EOM). Wavelength modulation can be performed by modulating the laser diode current, which allows for the high-frequency modulation but also results in the amplitude modulation, or by using the piezo-driven modulation, which supports the lower-frequency modulations without affecting the laser amplitude. Wavelength modulation is particularly useful for implementing the derivative spectroscopy techniques^{104,105}.

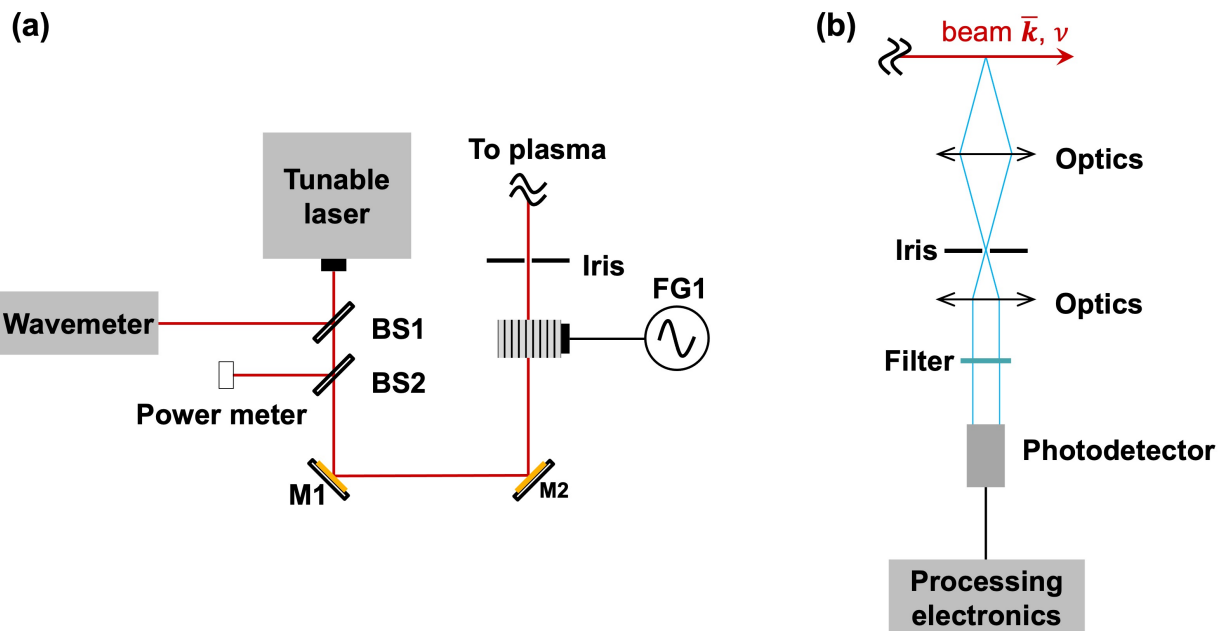


FIG. 8: Generalized LIF setup. a) Laser launch brunch, BS1,2 - are beam splitters, and M1,2 - mirrors. b) Detection branch. "Optics" can represent various combination of lenses arranged to collect fluorescent light.

The detection branch of the optical setup consists of a collecting lens that directs light through a series of lenses and a spatial filter (pinhole) into the detector. This lens is typically positioned so that its optical axis is perpendicular to the laser beam's wavevector, which enhances spatial resolution. The collected light is filtered around the fluorescence wavelength, either by a narrow bandpass filter or by a monochromator. Various detectors such as a photomultiplier tube (PMT), a photodiode, or a CCD camera can be used depending on the measurement requirements. For point measurements, a PMT is preferred due to its high sensitivity. A CCD camera is more suitable for planar LIF measurements. Additionally, the detection branch can be mounted on a movable stage, allowing measurements along the laser beam and enabling the acquisition of 1D distributions of parameters such as velocity and temperature.

Signal processing for the LIF measurements can be performed in various ways to achieve either time-

averaged or time-resolved information. A lock-in amplifier, synchronized with the laser modulation frequency, is commonly used. For more advanced techniques, utilizing beating frequencies help in the extraction of time-resolved information effectively. The photon-counting technique is also widely employed for this purpose. When the laser wavelength is modulated, the use of a lock-in amplifier to extract higher harmonics facilitates the derivation of the VDF profile. This technique provides a more sensitive analysis of the true VDF shape, particularly in cases of complex signals that deviate from a Maxwellian distribution.

The placement of the detection branch perpendicular to the laser beam typically necessitates at least two optical ports in the plasma chamber: one for the entry of the laser and another for collecting the LIF signal. However, modern industrial-scale plasma reactors are fully enclosed to ensure uniform processing of the materials and having more than one viewport can disrupt the plasma processes and alter the processing of the material. Additionally, space constraints often limit access to only one location around a plasma reactor. In such cases, confocal LIF is a suitable alternative. This technique allows both the input laser beam and the collected LIF signal to pass through the same axis into the plasma discharge, minimizing the need for multiple ports. Originally widespread in the fields of biology and medicine¹⁰⁶, confocal LIF has been adapted for TALIF and single LIF measurements across various scenarios^{107–110}. Recently, this method has been enhanced with structured laser light, specifically Laguerre-Gaussian beams, to improve the signal-to-noise ratio. This modification has been successfully implemented on a plasma source to measure the velocity of argon ions¹¹¹.

III. LIF/TALIF reference data

The microelectronics industry and sustainability applications use a combination of a wide variety of precursor gases such as CH₄, CF₄, CH₂F₂, CHF₃, C₂F₄, C₃F₆, C₄F₆, C₄F₈, NF₃, HBr, Cl₂, COS, SF₆, H₂, O₂, H₂O, N₂, He and Ar, among others to generate the plasma^{56,112–125}. It results in the generation of a combination of a wide variety of ions, radicals and metastable species that play different roles in the overall chemical process. The LIF/TALIF transitions to detect such species should be carefully selected such that there is no overlap in the excitation and fluorescence wavelengths of the species of interest with other species present in the detection volume. There are several species that have coincident excitation and fluorescence

wavelengths. Depending on the species present in the interrogation volume, the excitation and fluorescence wavelengths should be carefully examined to determine if a spectral filter or a monochromator is required for collecting fluorescence. While using a spectral filter for collecting fluorescence often provides a higher optical efficiency, the presence of overlapping fluorescence might necessitate the use of a monochromator to obtain the wavelength of the fluorescence and differentiate between the interfering species. For example, in an industrial scale silicon etching CCP discharge with argon and oxygen admixture, we found that both the excitation and the fluorescence wavelengths of O_2^+ ions and SiO radicals coincide with one another inhibiting the differentiation between the two species even with the use of a monochromator. This reference data is intended to assist in the selection of the LIF/TALIF transitions that do not overlap with other species present in the interrogation volume. Some groups of species with overlapping excitation and fluorescence wavelengths that may not be differentiable by the use of a spectral filter are listed below:

1. NO, NS, O_2 , O_2^+ and SiO.
2. CH_3O , OH, SiCl, SiF, Ti and W.
3. CF_3O , CN_2 , C_2H_3O , C_2H_5O , HC_2O , N_2O^+ and SH.
4. CH_2O and CN.
5. C_2H_5S , C_3H_7S and N_2^+ .
6. C_2H_5S , C_3H_7S and SiN.
7. C_2H_5S , C_3H_7S , CS_2^+ , HC_2S_2 and HSiF.
8. Br_2^+ , CuSH and Na_2 .
9. NO_3 and RuO.
10. BO_2 and Br_2 .
11. CH_2 , C_2O and NH_2 .
12. SiCCl and SiCF.

13. SiCCl and TiC.
14. CH₂ and C₂O.
15. C₂O and HNO.
16. C₂P, C₂S, HBF, SiCl₃O and SiC₃H.

A compiled list of available LIF/TALIF transitions for atomic, molecular, ionic, and metastable species relevant to the microelectronics industry and sustainability applications are shown in tables I, II, III, IV, V, VI, VII and VIII. Several of these transitions were studied a few decades ago when the availability and the use of equipment such as iCCD cameras or a monochromator were unavailable. When the transition/fluorescence information was unavailable, a "not-reported" (*NR*) indication was mentioned in the tables. Certain neutral molecules cannot be detected by excitation from the ground state and require the presence of higher vibrational states for their detection. They have been marked in the tables. While we have put efforts into reporting all the relevant species that have been reported in the literature, it is possible that the reported tables inadvertently omitted relevant species/transitions that have been previously reported.

Sl. No.	Species	Transition	Excitation (nm)	Fluorescence (nm)	Reference
1	AlO	$B^2\Sigma^+ - X^2\Sigma^+$	464–470	507–519	126–128
2	AlS	$A^2\Sigma^+ - X^2\Sigma^+$	418 – 430	440	129
3	As ₂	$A^1\Sigma_u^+ - X^1\Sigma_g^+$	240 – 241	275 – 305	130–132
		$A^1\Sigma_u^+ - X^1\Sigma_g^+$	248	289.3	131
4	BC	$B^4\Sigma^- - X^4\Sigma^-$	557.4 – 559.2	596.9	133,134
		$E^4\Pi - X^4\Sigma^-$	290.9 – 291.5	<i>NR</i>	134
5	BCl	$A^1\Pi - X^1\Pi^+$	272	278	135
6	BH	$A^1\Pi - X^1\Sigma^+$	396	429 – 434	136,137
7	BH ₂	$\tilde{A}^2B_1(\Pi_u) - \tilde{X}^2A_1$	727.2 – 742.4	<i>NR</i>	138
8	BO	$A^2\Pi - X^2\Sigma^+$	313.5 – 316.5, 422 – 428, 434.5	<i>NR</i>	139,140
9	BO ₂	$A^2\Pi_u - X^2\Pi_g$	434 – 434.3	<i>NR</i>	139
		<i>NR</i>	545.6, 547.1	574 – 586	141
		$A^2\Pi_u - X^2\Pi_g$	579 – 583	538–554, 571 – 587, 611 – 627, 630 – 646	142
10	BS ₂	$\tilde{A}^2\Pi_u - \tilde{X}^2\Pi_g$	530 – 760	424 – 486	143
11	Br ₂	$B^3\Pi_{0+u} - X^1\Sigma_g^+$	548 – 595	618 – 621, 714 – 1110	144,145
12	c-C ₆ H ₇	$\tilde{A}^2A_2 - \tilde{X}^2B_1$	549.5 – 549.9	<i>NR</i>	146
13	CBr ₂	$\tilde{A}^1B_1 - \tilde{X}^1A_1$	561 – 575	588 – 672	147,148
14	CCl	$A^2\Delta - X^2\Pi$	278	<i>NR</i>	149,150
15	CCl ₂	$A^1B_1 - X^1A_1$	416 – 556	391 – 500, >580	151–156
16	CCl ₂ S	$\tilde{B} - \tilde{X}$	274 – 297	<i>NR</i>	157
17	CF	$A^2\Sigma^+ - X^2\Pi$	223.8	230.6	158
18	CF ₂	$\tilde{A} - \tilde{X}$	260 – 276	260 – 390	159–161
19	CF ₃ O	$\tilde{A}^2A_1 - \tilde{X}^2E$	332 – 352	355 – 400	162,163
20	CF ₃ S	$\tilde{A}^2A_1 - \tilde{X}^2E_{3/2}$	373.8 – 374, 377.7 – 377.8, 365.8 – 366	<i>NR</i>	162
21	CFBr	$\tilde{A}^1A'' - \tilde{X}''A''$	422.6 – 424.8	416 – 556	164,165
22	CFCl	$\tilde{A} - \tilde{X}$	363.3, 367.3, 372.7, 378.3, 384	330 – 395	151,155,166
23	CH	$A^2\Delta - X^2\Pi$	431	489	167
		$A^2\Delta - X^2\Pi$	427.9 – 428.1, 435.4 – 435.8	485	82,168
		$B^2\Sigma^- - X^2\Pi$	363.3 – 363.6, 387 – 388	385 – 415, 423 – 435, 443 – 460	168–170

TABLE I: Laser-induced fluorescence transitions of neutral molecular species - 1. *NR*: not reported.

Sl. No.	Species	Transition	Excitation (nm)	Fluorescence (nm)	Reference
24	CHF	$\tilde{A}^1 A'' - \tilde{X}^1 A'$	492 - 493, 514.5, 574 - 582	515 - 521, 550 - 570, 600 - 620, 650 - 670	171-177
25	CH ₂	$\tilde{b}^1 B_1 - \tilde{a}^1 A_1$	589 - 595	635 - 651	178
26	CH ₂ O	$\tilde{A}^1 A_2 - \tilde{X}^1 A_1$	352 - 357	380 - 550	179,180
27	CH ₃ O	$A^2 A_1 - X^2 E$	270 - 330	300 - 400	181-185
		$\tilde{B} - \tilde{X}$	357 - 376	316 - 375	186
28	CH ₃ S	$\tilde{A}^2 A_1 - \tilde{X}^2 E$	364 - 378	370 - 500	187,188
29	CN	$B^2 \Sigma - X^2 \Sigma$	356.5, 381 - 388.5, 565 - 610	388.8, 389.5	63,189-191
30	CN ₂	$^3 \Pi_1 - ^3 \Sigma^-, \tilde{A}^3 \Pi - \tilde{X}^3 \Sigma^-$	327 - 336	330 - 440	192-194
31	CO	$B^1 \Sigma^+ - X^1 \Sigma^+$	2 × 230.1	484	195
32	CO ₂	(00 ⁰ 0) - (10 ⁰ 01)	2005, 2700	4260 - 4270	196,197
33	CS	$A^1 \Pi - X^1 \Sigma^+$	257.5 - 258.3	250 - 290	198-200
34	CS ₂	$V^1 B_2 - \tilde{X}^1 \Sigma_g^+$	280 - 338	370, 380, 403.7	201-204
35	CuSH	$\tilde{A}^1 A'' - \tilde{X}^1 A'$	472 - 515	480 - 506	205
36	Cu ₂	$A^1 \Sigma_u^+ - X^1 \Sigma_g^+$	490.27	495 - 499	65
		$B^1 \Pi_u - X^1 \Sigma_g^+$	449.8	460.7	206
37	C ₂	$d^3 \Pi - a^3 \Pi$	516	563	81
		$d - a$	470	425 - 438	82,207
		$A^1 \Pi_u - X^1 \Sigma_g^+$	690.9	790.8	208-210
		$d^3 \Pi_g - a^3 \Pi_u$	516.5	559	208,211
38	C ₂ H ₂	$\tilde{A} - \tilde{X}$	225 - 235	250 - 360	212
39	C ₂ H ₃ O	$\tilde{B}^2 A'' - \tilde{X}^2 A''$	330 - 350	340 - 420	213-215
40	C ₂ H ₃ S	$\tilde{B} - \tilde{X}^2 A''$	458.2 - 458.5	464 - 531	216
41	C ₂ H ₅ O	$\tilde{A} - \tilde{X}$	310 - 350	340 - 430	181,182,217
42	C ₂ H ₅ S	$\tilde{A} - \tilde{X}$	390 - 450	420 - 580	218
		$\tilde{B}^2 A' - \tilde{X}^2 A''$	397 - 427	352 - 425	219
43	C ₂ N	$\tilde{A}^2 \Delta - \tilde{X}^2 \Pi$	465.8, 470 - 471.5	466 - 580	220,221
44	C ₂ O	$\tilde{A}^3 \Pi_i - \tilde{X}^3 \Sigma^-$	588 - 685	650 - 780	222
45	C ₂ P	$^2 \Delta_i - \tilde{X}^2 \Pi_r$	596 - 633	556 - 627	223
46	C ₂ S	$\tilde{A}^3 \Pi_i \leftarrow \tilde{X}^3 \Pi^-$	675 - 690, 604 - 614	553 - 614	224
47	C ₃	$A^1 \Pi_u - X^1 \Sigma_g^+$	405.3	398 - 411	225
		$A - X$	425 - 430	405	82
48	C ₃ H ₇ S	$\tilde{A} - \tilde{X}$	395 - 430	420 - 520	226
49	C ₃ N	$\tilde{B}^2 \Pi_i - \tilde{X}^2 \Sigma^+$	343 - 350	284 - 336	227
50	C ₄ H	$\tilde{B}^2 \Sigma^+ - \tilde{X}^2 \Sigma^+$	400 - 416.7	> 420	228
51	FCO	$\tilde{A}^2 \Pi - \tilde{X}^2 A'$	307 - 345	333 - 477	229
52	GaCl	$A^3 \Pi_0^+ - X^1 \Sigma^+$	332 - 346	364	131
53	HBF	$\tilde{A}^2 A'' \Pi - \tilde{X}^2 A'$	602 - 666	535 - 628	230
54	HBr	$M^1 \Pi - X^1 \Sigma^+$	115.2 - 116.2	<i>NR</i>	231
55	HCB _r	$\tilde{A} - \tilde{X}^2 \tilde{0}$	560 - 561.3	468 - 528	148

TABLE II: Laser-induced fluorescence transitions of neutral molecular species - 2. *NR*: not reported.

Sl. No.	Species	Transition	Excitation (nm)	Fluorescence (nm)	Reference
56	HCl	$V^1\Sigma^+ - X^1\Sigma^+$	115.7 - 115.9	<i>NR</i>	231
57	HCO	$^2\tilde{A}' - ^2\tilde{A}''$	613 - 618	638 - 664	232
58	HC ₂ O	$X^2A' - ^2A''$	310 - 360	350 - 460	233
59	HC ₂ S ₂	$\tilde{B}^2A'' - \tilde{X}^2A''$	435 - 458	458 - 530	234
60	HC ₄ S	$\tilde{A}^2\Pi_{3/2} - \tilde{X}^2\Pi_{3/2}$	487 - 501	426 - 488	235,236
61	HC ₆ S	$^2\Pi_{3/2} - ^2\Pi_{3/2}$	572 - 590	<i>NR</i>	237
62	HNO	$\tilde{A}^1A'' - \tilde{X}^1A''$	623 - 626, 641.6 - 643	685 - 780	238-240
63	HSiBr	$\tilde{A}'A'' - \tilde{X}^1A^1$	458 - 503	<i>NR</i>	241
64	HSiCl	$\tilde{A}'A'' - \tilde{X}^1A'$	444 - 485, 538 - 550	471, 483, 489, 503, 524	242-244
65	HSiF	$\tilde{A}^1A'' - \tilde{X}^1A'$	430, 446.5	425 - 530	245,246
66	HSiNC	$\tilde{A}^1A'' - \tilde{X}^1A'$	499.75 - 502	428.2, 444.3, 461.9, 480.6	247
67	HSiNCO	$\tilde{A}^1A'' - \tilde{X}^1A'$	490 - 492	379.6 - 477.51	248
68	HSO	$\tilde{A} - \tilde{X}$	539 - 540, 585, 600 - 615, 625 - 645	> 665	238,249-251
69	HSnCl	$\tilde{A}^1A'' - \tilde{X}^1A'$	455 - 500	389 - 482	252
70	H ₂	$E, F^1\Sigma_g^+ - X^1\Sigma_g^+$	2×193.3	750, 830	253
	H ₂ ††	$B^1\Sigma_g^+ - X^1\Sigma_g^+$	106.2 - 106.7	<i>NR</i>	254-256
71	InCl	$A^3\Pi_0^+ - X^1\Sigma^+, B^3\Pi_1 - X^1\Sigma^+$	340 - 360	363.7	131
72	IO	$A^2\Pi_{3/2} - X^2\Pi_{3/2}$	435 - 468	500 - 600	257,258
73	I ₂	$B^3\Pi_{0u}^+ - X^1\Sigma_g^+$	501.7, 514.5	515 - 830	259-261
74	KH	$A^1\Sigma^+ - X^1\Sigma^+$	502.4 - 504	548.5 - 557.5	262
75	K ₂	$B^1\Pi_u - X^1\Sigma_g^+$	632.8	633 - 650	263
		$C^1\Pi_u - X^1\Sigma_g^+$	420 - 435, 457.9	420 - 475, 550 - 580	264,265
76	NaK	$D^1\Pi - X^1\Sigma^+$	476 - 529	1052 - 2500	266
77	Na ₂	$B^1\Pi_u - X^1\Sigma_g^+$	465.7 - 514.5	470 - 540	267
78	NCO	$A - X$	420 - 440	465	268
79	NC ₃ O	$^2\Sigma - ^2\Sigma$	365.7 - 365.9	329 - 365	269
		$^2\Pi - ^2\Pi$	365.6 - 365.8	329 - 365	269
80	NC ₃ S	$\tilde{A}^2\Pi_{3/2} - \tilde{X}^2\Pi_{3/2}$	463.9 - 464.1	408 - 455	270
81	NF	$b' \Sigma - X^3\Sigma^-$	530	528.9	271
82	NH	$A^3\Pi - X^3\Sigma^-$	303 - 305, 329 - 336	330 - 345	62,272-274
83	NH ₂	$\tilde{A}^2A_1 - \tilde{X}^2B_1$	571 - 662.2	516 - 824	268,275,276
84	NH ₃	$X - C'$	2×305	550 - 575, 720	277
85	N ₃	$\tilde{A}^2\Sigma^+ - \tilde{X}^2\Pi_{3/2}$	271.9	271.1 - 272.8	278

TABLE III: Laser-induced fluorescence transitions of neutral molecular species - 3. *NR*: not reported. ††: Laser excitation is from a vibrationally/rotationally excited state of a neutral gas molecule.

Sl. No.	Species	Transition	Excitation (nm)	Fluorescence (nm)	Reference
86	NO	$A^2 \Sigma^- - X^2 \Pi$	226 – 227	248	279–281
		$D^2 \Sigma^- - X^2 \Pi$	193	196 – 226	282
	NO ††	$C^2 \Sigma^- - X^2 \Pi$	193	208	282
87	NO ₂	$\tilde{X}^2 A_1 - \tilde{A}^2 B_2$	434.9, 430.6, 435.1	638 – 663	283
88	NO ₃	$\tilde{B}^2 E' - \tilde{X}^2 A'_2$	500 – 680	464 – 662	284,285
89	NS	$C^2 \Sigma^+ - X^2 \Pi$	230 – 232	236 – 238	286
		NR	300 – 310, 360 – 370	NR	287
90	O ₂ ††	$B^3 \Sigma_u^- - X^3 \Sigma_g^-$	223 – 226	240 – 440	288
91	OH	$X - A$	280 – 286	304 – 314	73,289
92	PbF	$A^2 \Sigma_{1/2}^+ - X^2 \Pi_{1/2}$	260 – 285	NR	290,291
		$B^2 \Sigma^+ - X^2 \Pi_{1/2}$	426 – 450	435 – 500, 700 – 800, 1200 – 1300	292
93	P ₂	NR	193	322.2	131
94	PH ₂	$\tilde{A}^2 A_1 - \tilde{X}^2 B_1$	419 – 547	430 – 555	293–295
95	PO	$B^2 \Sigma^+ - C^2 \Pi$	324	NR	296
		$A^2 \Sigma^+ - X^2 \Pi_{1/2}$	245.6 – 246.6	239 – 279, 319 – 359	297
		$A^2 \Sigma^+ - X^2 \Pi_{3/2}$	247 – 247.8	239 – 279, 319 – 359	297
96	RuB	$[18.4]2.5 - X^2 \Delta_{5/2}$	522 – 524, 542 – 543	NR	298
97	RuC	$[18.1]^1 \Pi_1 - X^1 \Pi^+, [5.7]^1 \Delta_2$	431 – 439, 552.9	553, 806	299
98	RuCl	$^4 \Gamma_{5.5} - X^4 \phi_{4.5}$	508 – 557	499 – 546	300
		$^4 \phi_{4.5} - X^4 \phi_{4.5}$	426 – 569	430 – 442	
99	RuF	$[18.2]^4 \Gamma_{4.5} - X^4 \phi_{3.5}$	450 – 452	410 – 441	300
			545 – 548	470 – 533	
			758 – 764	697 – 732	
100	RuN	$(0,0)F^2 \Sigma^+ - X^2 \Sigma^+$	529.6 – 532	NR	301
101	RuO	$[18.1]4 - X^5 \Delta_4$	529.5 – 531	463 – 503	300
102	SH	$^2 \Sigma^+ - ^2 \Pi_{3/2,1/2}$	323 – 330	320 – 362	302–304
103	SiBr	$B^2 \Sigma - X^2 \Pi_r$	308	296 – 304	305,306
104	SiCCl	$\tilde{A}^2 \Sigma^+ - \tilde{X}^2 \Pi$	550 – 615	545 – 650	307
105	SiCF	$\tilde{A}^2 \Sigma^+ - \tilde{X}^2 \Pi$	574 – 604	547 – 596	308
106	SiCH	$\tilde{A}^2 \Sigma^+ - \tilde{X}^2 \Pi_i$	650 – 680, 700 – 740	NR	309

TABLE IV: Laser-induced fluorescence transitions of neutral molecular species - 4. NR : not reported. ††: Laser excitation is from a vibrationally/rotationally excited state of a neutral gas molecule..

Sl. No.	Species	Transition	Excitation (nm)	Fluorescence (nm)	Reference
107	SiCl	$B^2 \Sigma - X^2 \Pi$	275, 295, 308	280, 320, 290 – 307	305,310
108	SiCl ₂	$\tilde{A}^1 B_1 - \tilde{X}^1 A_1$	309 – 333	331 – 390	311
109	SiCl ₃ O	$\tilde{A}^2 A_1 - \tilde{X}^2 E$	590 – 650	617 – 653	312
110	SiC ₃ H	$\tilde{A}^2 \Sigma^+ - \tilde{X}^2 \Pi_i$	613 – 681	578 – 663	313
111	SiF	$X - B$	288	308 – 315	314
112	SiF ₂	$X - A$	221.6	234 – 244	314
113	SiH	$A^2 \Delta - X^2 \Pi$	409 – 416	413	45,315–317
114	SiH ₂	$\tilde{A}^1 B - \tilde{X}^1 A$	579.2 – 580.4	618	318–320
115	SiN	$\tilde{B}^2 \Sigma - \tilde{X}^2 \Sigma$	396	414	321
116	SiO	$A^1 \Sigma - X^1 \Sigma$	220 – 237	214 – 350	48,322,323
117	SO	NR	248.1, 248.7	250 – 450	324
118	SO ₂	NR	248.1, 248.7	250 – 450	324
		$\tilde{X}(^1 A_1) - \tilde{C}(^1 B_2), \tilde{B}(^1 B_1), \tilde{A}(^1 A_2)$	266	250 – 350	325
119	S ₂	$B^3 \Sigma_u^- - X^3 \Sigma_g^-$	325, 337	310 – 410	326
120	S ₂ O	$\tilde{C}^1 A' - \tilde{X}^1 A'$	340	NR	238,327
121	TaC	$[18.61]^2 \Pi_{3/2} - X^2 \Sigma^+, NR$	537.1 – 537.8, 505.2	401 – 509	328
122	TiC	$^1 \Pi - X^3 \Sigma^+$	606.9 – 608.3	538 – 603	329
		$^1 \Pi - a^1 \Sigma^+$	619.8 – 621.6	NR	
		$^1 \Pi - b^1 \Sigma^+$	690.4 – 691.5	NR	
		$^1 \Pi - c^1 \Sigma^+$	664.5 – 665.5	NR	
123	TiF	$[37.8]^4 \Phi - X^4 \Phi$	250.9 – 255.4	NR	330
		$^4 \Delta - X^4 \Phi$	249.5 – 250.1	NR	330

TABLE V: Laser-induced fluorescence transitions of neutral molecular species - 5. NR : not reported.

Sl. No.	Species	Transition	Excitation (nm)	Fluorescence (nm)	Reference
1	Al	${}^2P_{3/2}^0 - {}^2D_{5/2}$	309.3	394.4, 396.2	331
		${}^3P_{1/2} - {}^4S_{1/2}$	394.4	396.2	332
2	As	$4s^3 {}^4S_{3/2} - 5s {}^4P_{3/2}$	193.8	245	333
3	B	$2s^2 2p {}^2P_{3/2}^0 - 2s^2 3s {}^2S_{1/2}$	249.7, 249.8	209, 206.7	334
		$2s^2 2p {}^2P_{3/2}^0 - 2s 2p^2 {}^2D_{3/2,5/2}$	208.96	208.96	335
4	Br	$4p^5 {}^2P_{3/2}^0 - 5p {}^4S_{3/2}^0$	2×252.59	635	336
5	C	$2p 3p {}^3P - 2p^2 {}^3P$	2×280	910	337
6	Cl	$3p^5 {}^2P^0 - 4p {}^4S^0$	2×233.2	725 – 775	47,338,339
7	Cr	$3d^5 4p^7 P_J - 3d^5 4s^7 S_3$	425.4	427.5, 429	340
8	Cu	$4s^2 S_{1/2} - 4p^2 P_{3/2}^0$	324.8	510.6, 570	341
9	F	$2p^5 {}^2P^0 - 3p {}^2D^0$	170	776	46
10	Fe	$3d^6 4s^2 a {}^5D_4 - 3d^7 ({}^4F) 4p y {}^5F_5^0$	296.7	373.5	342
		$3d^6 4s^2 a {}^5D_4 - 3d^7 ({}^4F) 4p y {}^5D_4^0$	302.06	382.04	343
11	Ga	$4^2D_{3/2} - 4^2P_{1/2}, {}^5S_{1/2} - 4^2P_{3/2}$	287.4, 403.3	294.4, 417.2	344
12	H	$1s^2 S - 3d {}^2D$	2×205	656.3	66
13	I	$5p^5 {}^2P^0 - {}^2D^0$	2×304.7	178.3	345
14	Kr	$4p^6 {}^1S_0 - 5p'[3/2]_2$	2×204.1	587, 826.3	66
15	N	$2p^3 {}^4S^0 - 3p {}^4D^0$	2×211	870, 822, 744	66
16	Na	<i>NR</i>	2×685	818	346
		${}^2P_{1/2}, {}^2P_{3/2} - {}^2S_{1/2}$	589	<i>NR</i>	347,348
17	O	$2p^4 {}^3P - 3p {}^3P$	2×225.7	844.9, 777	66
18	Pb	$6s^2 6p^2 {}^3P_0 - 6s^2 6p(2P_{0.5}^0) 7s {}^3P_1^0$	283.31	405.78	349
19	S	$3p^4 {}^3P - 4p {}^3P$	2×288	VUV	350
20	Si	$3p^2 {}^3P_0 - 4s {}^3P_1^0$	251.4	252.8	351
21	Ti	$3d_2 4s 4p - 3d_2 4s_2 ({}^3F_3)$	322.3	511.3	352
		${}^3D_{1,2,3}, {}^1F_3, {}^3F_3, {}^3G_3 - {}^3F_{2,3,4}$	221 – 296	250 – 341	353
22	W	$5d^4 6s^2 {}^5D_0 - 5d^5 {}^4D 6s_1^0$	287.9	302.5	354,355
23	Xe	$5p^6 {}^1S_0 - 7p[3/2]_2$	2×225.5	462.6	66

TABLE VI: Laser-induced fluorescence transitions of neutral atomic species. *NR*: not reported.

Sl. No.	Species	Transition	Excitation (nm)	Fluorescence (nm)	Reference
1	Ar ⁺ *	$3d^4 F_{9/2} - 4p^4 F_{7/2}$	664.4	434.8	356
		$3d^4 F_{7/2} - 4p^4 D_{5/2}$	668.6	442.7	96,357-363
		$4p^2 D_{5/2} - 4s^2 P_{3/2}$	488	422.8	84
		$4p' \ ^2F_{7/2}^0 - 3d' \ ^2G_{9/2}$	611.7	461.1	364
2	Br ₂ ⁺	$^2\Pi_u - X^2\Pi_g$	472.7	480 – 640	365
3	Cl ⁺ *	$^5P_3 - ^5D_4^0$	542.3	479.5	366
4	Cl ₂ ⁺	$X^2\Pi_i - A^2\Pi_i$	387.6	396	367
5	CS ₂ ⁺	$X^2\Pi_{3/2} - A^2\Pi_{3/2}$	427 – 476	460 – 550	368
		$A^2\Pi_u - X^2\Pi_g$	410 – 480	507.7	369
6	C ₂ S ₂ ⁻	$^2\Pi_{3/2} - ^2\Pi_{3/2}$	542.5 – 543	555 – 695	370
7	I ⁺ *	$^5D_4^0 - ^5P_3$	696.1	516.3	371
8	Kr ⁺ *	$4d^4 F_{7/2} -$	820.3	462.9	372
		$5d^4 F_{7/2} -$	729	473.9	373
9	La ⁺ *	$5d6s \ a^3D_1 - 5d6p \ y^3D_2^0$	403.2	379.1	374
10	N ₂ ⁺	$B^2 \ \Sigma_u^+ - X^2\Sigma_g^+$	391	428	43
			330	458.8	375
11	N ₂ O ⁺	$\tilde{A}^2\Sigma^+ - \tilde{X}^2\Pi_i$	337 – 356	312 – 345	376
12	O ₂ ⁺	$X^2\Pi_g - A^2\Pi_u$	225 – 227	245	377
13	SiO ⁺	$B^2\Sigma^+ - X^2\Sigma^+$	385	383 – 385	378
14	Ti ⁺	$3d_2 \ 4p(z^4G_{5/2}^0) - 3d_2 \ 4s(a^4F_{3/2})$	338.4	486.6	352
15	Xe ⁺ *	$5d^4 F_{5/2} - 6p^4 D_{5/2}$	834.7	541.9	59
		$6p^4 P_{5/2}^0 - 5d^4 D_{7/2}$	605.1	529.2	379,380
		$6p^4 D_{5/2}^0 - 5d^4 F_{7/2}$	680.6	492.2	44

TABLE VII: Laser-induced fluorescence transitions of metastable and ground states of ionic species.

Sl. No.	Species	Transition	Excitation (nm)	Fluorescence (nm)	Reference
1	Ar*	$3p^5P_{1/2} - 4p^5D_{3/2}$	696.7	826.7	95
		$3p^5S_{1/2} - 4p^5P_{1/2}$	772.6	810.6, 826.7	381
		$1s_5 - 2p_9$	811.5, 810.4	811.5, 772.6	382
		$1s_2 - 2p_3$	841.1	706.9	383
		$1s_2 - 2p_3$	842.5	842.5, 801.7	384
		$3d^4F_{(7/2)} - 4p^4D_{(3/2)}$	667.9	750.6	362,363
2	F*	$^4D_{5/2}^0 - ^4P_{3/2}$	690.3	677.4	385
3	He*	$3^3P - 2^3S$	388.9	706.5, 587.6	386
		$2^1S - 3^1P$	501.6	667.8	386
4	He ₂ *	$a^3\Sigma_u^+ - d^3\Sigma_u^+$	2 × 940	640	387
5	Kr*	$5s[3/2]_2^0 - 5p[3/2]_2$	760.2	819	388,389
		$5s[3/2]_2 - 5p[5/2]_2$	810.44	877.6	388
6	N ₂ *	$A^3\Sigma_u^+ - B^3\Pi_g$	687.44, 618	762, 676	390,391
7	P*	$3s^23p^3\ ^2P_{1/2,3/2}^0 - 3s^23p^2(^3P)4s\ ^2P_{3/2}$	253.4, 253.6	213.6, 213.6	392,393
8	Xe*	$6s^2[1/2]_1^0 - 6p^2[3/2]_1^0$	834.7	473.4	59,394
		$6s[3/2]_2^0 - 6p[3/2]_2$	823.2	823.2	394,395

TABLE VIII: Laser-induced fluorescence transitions of neutral metastable species.

IV. Summary

Laser-induced fluorescence provides both spatial and temporally resolved characteristics of the neutral species, the plasma-produced radicals, ions, and metastables. It is a useful tool that enables direct measurement of densities, ion velocities, and temperatures. LIF can help in the validation of simulation models and help in the development of the predictive capabilities of plasma-material interactions. In this report, we have reviewed the basic principles of LIF, the widely used types of LIF setups and compiled a list of the available transitions to generate a reference data for laser-induced fluorescence transitions relevant in the microelectronics industry and the sustainability applications. We have identified the groups of species with overlapping LIF/TALIF excitation and fluorescence wavelengths. This compilation intends to assist in the identification of the possible species that can be detected by LIF/TALIF an interrogation volume.

V. Acknowledgements

This work was performed under the U.S. Department of Energy through contract DE-AC02-09CH11466. The authors would like to thank Shahid Rauf, Alexandre Likhanskii, Prashanth Kothnur, Guus Reefman, and Mu-Chien Wu for their feedback and input in providing gases relevant to processing applications.

VI. Data Availability

Data sharing is not applicable to this article as no new data were created or analyzed in this study.

VII. Conflict of Interest

The authors have no conflicts to disclose.

VIII. References

¹M. M. Waldrop, "The chips are down for moore's law," Nature News **530**, 144 (2016).

- ²M. S. Lundstrom and M. A. Alam, “Moore’s law: The journey ahead,” *Science* **378**, 722–723 (2022).
- ³J. Shalf, “The future of computing beyond Moore’s Law,” *Philosophical Transactions of the Royal Society A* **378**, 20190061 (2020).
- ⁴T. N. Theis and H.-S. P. Wong, “The end of moore’s law: A new beginning for information technology,” *Computing in science & engineering* **19**, 41–50 (2017).
- ⁵D. B. Graves, “Plasma processing,” *IEEE transactions on Plasma Science* **22**, 31–42 (1994).
- ⁶I. Adamovich, S. Agarwal, E. Ahedo, L. L. Alves, S. Baalrud, N. Babaeva, A. Bogaerts, A. Bourdon, P. Bruggeman, C. Canal, *et al.*, “The 2022 plasma roadmap: low temperature plasma science and technology,” *Journal of Physics D: Applied Physics* **55**, 373001 (2022).
- ⁷G. N. Parsons and R. D. Clark, “Area-selective deposition: Fundamentals, applications, and future outlook,” *Chemistry of Materials* **32**, 4920–4953 (2020).
- ⁸H. C. Knoops, T. Faraz, K. Arts, and W. M. Kessels, “Status and prospects of plasma-assisted atomic layer deposition,” *Journal of Vacuum Science & Technology A: Vacuum, Surfaces, and Films* **37**, 030902 (2019).
- ⁹G. Oehrlein, D. Metzler, and C. Li, “Atomic layer etching at the tipping point: an overview,” *ECS Journal of Solid State Science and Technology* **4**, N5041 (2015).
- ¹⁰L. Dorf, J.-C. Wang, S. Rauf, Y. Zhang, A. Agarwal, J. Kenney, K. Ramaswamy, and K. Collins, “Atomic precision etch using a low-electron temperature plasma,” in *Advanced Etch Technology for Nanopatterning V*, Vol. 9782 (SPIE, 2016) pp. 30–37.
- ¹¹A. V. Jagtiani, H. Miyazoe, J. Chang, D. B. Farmer, M. Engel, D. Neumayer, S.-J. Han, S. U. Engelmann, D. R. Boris, S. C. Hernández, *et al.*, “Initial evaluation and comparison of plasma damage to atomic layer carbon materials using conventional and low t_e plasma sources,” *Journal of Vacuum Science & Technology A* **34** (2016).
- ¹²S. Rauf, A. Balakrishna, A. Agarwal, L. Dorf, K. Collins, D. R. Boris, and S. G. Walton, “Three-dimensional model of electron beam generated plasma,” *Plasma Sources Science and Technology* **26**, 065006 (2017).
- ¹³L. Dorf, R. Dhindsa, J. Rogers, D. S. Byun, E. Kamenetskiy, Y. Guo, K. Ramaswamy, V. N. Todorow, O. Luere, C. Linying, *et al.*, “Plasma processing assembly using pulsed-voltage and radio-frequency power,” (2022), uS Patent 11,462,388.
- ¹⁴L. Dorf, R. Dhindsa, J. Rogers, D. S. Byun, E. Kamenetskiy, Y. Guo, K. Ramaswamy, V. N. Todorow, and O. Luere, “Plasma processing using pulsed-voltage and radio-frequency power,” (2022), uS Patent App. 17/315,234.
- ¹⁵L. Zhang, “Silicon process and manufacturing technology evolution: An overview of advancements in chip making,” *IEEE Consumer Electronics Magazine* **3**, 44–48 (2014).
- ¹⁶K. Bera, S. Rauf, J. Forster, and K. Collins, “Self-organized pattern formation in radio frequency capacitively coupled discharges,” *Journal of Applied Physics* **129** (2021).
- ¹⁷G. Cunge, M. Kogelschatz, O. Joubert, and N. Sadeghi, “Plasma-wall interactions during silicon etching processes in high-density HBr/Cl₂/O₂ plasmas,” *Plasma Sources Science and Technology* **14**, S42 (2005).

- ¹⁸M. Badaroglu, “International roadmap for devices and systems,” More Moore: <https://irds.ieee.org/roadmap-2017> (2017).
- ¹⁹M. Atature, D. Englund, N. Vamivakas, S.-Y. Lee, and J. Wrachtrup, “Material platforms for spin-based photonic quantum technologies,” *Nature Reviews Materials* **3**, 38–51 (2018).
- ²⁰F. A. Zwanenburg, A. S. Dzurak, A. Morello, M. Y. Simmons, L. C. Hollenberg, G. Klimeck, S. Rogge, S. N. Coppersmith, and M. A. Eriksson, “Silicon quantum electronics,” *Reviews of modern physics* **85**, 961 (2013).
- ²¹T. D. Ladd, F. Jelezko, R. Laflamme, Y. Nakamura, C. Monroe, and J. L. O’Brien, “Quantum computers,” *Nature* **464**, 45–53 (2010).
- ²²S. Samukawa, M. Hori, S. Rauf, K. Tachibana, P. Bruggeman, G. Kroesen, J. C. Whitehead, A. B. Murphy, A. F. Gutsol, S. Starikovskaia, *et al.*, “The 2012 plasma roadmap,” *Journal of Physics D: Applied Physics* **45**, 253001 (2012).
- ²³I. Adamovich, S. Baalrud, A. Bogaerts, P. Bruggeman, M. Cappelli, V. Colombo, U. Czarnetzki, U. Ebert, J. G. Eden, P. Favia, *et al.*, “The 2017 Plasma Roadmap: Low temperature plasma science and technology,” *Journal of Physics D: Applied Physics* **50**, 323001 (2017).
- ²⁴M. G. Kong, G. Kroesen, G. Morfill, T. Nosenko, T. Shimizu, J. Van Dijk, and J. Zimmermann, “Plasma medicine: an introductory review,” *new Journal of Physics* **11**, 115012 (2009).
- ²⁵P. Ranieri, N. Sponsel, J. Kizer, M. Rojas-Pierce, R. Hernández, L. Gatiboni, A. Grunden, and K. Stapelmann, “Plasma agriculture: Review from the perspective of the plant and its ecosystem,” *Plasma Processes and Polymers* **18**, 2000162 (2021).
- ²⁶Q. Chen, J. Li, and Y. Li, “A review of plasma–liquid interactions for nanomaterial synthesis,” *Journal of Physics D: Applied Physics* **48**, 424005 (2015).
- ²⁷A. Bogaerts, X. Tu, J. C. Whitehead, G. Centi, L. Lefferts, O. Guaitella, F. Azzolina-Jury, H.-H. Kim, A. B. Murphy, W. F. Schneider, *et al.*, “The 2020 plasma catalysis roadmap,” *Journal of Physics D: Applied Physics* **53**, 443001 (2020).
- ²⁸J. C. Whitehead, “Plasma–catalysis: the known knowns, the known unknowns and the unknown unknowns,” *Journal of Physics D: Applied Physics* **49**, 243001 (2016).
- ²⁹A. Vardelle, C. Moreau, N. J. Themelis, and C. Chazelas, “A perspective on plasma spray technology,” *Plasma Chemistry and Plasma Processing* **35**, 491–509 (2015).
- ³⁰S. M. Starikovskaia, “Plasma assisted ignition and combustion,” *Journal of Physics D: Applied Physics* **39**, R265 (2006).
- ³¹Y. Huang, S. Li, Q. Zheng, X. Shen, S. Wang, P. Han, Z. Liu, and K. Yan, “Recent progress of dry electrostatic precipitation for PM2.5 emission control from coal-fired boilers,” *Int. J. Plasma Environ. Sci. Technol* **9**, 69–95 (2015).
- ³²S. Nijdam, E. Van Veldhuizen, P. Bruggeman, and U. Ebert, “An introduction to nonequilibrium plasmas at atmospheric pressure,” *Plasma chemistry and catalysis in gases and liquids*, 1–44 (2012).
- ³³Y.-S. Byeon, E. J. Hong, S. Yoo, T. Lho, S.-Y. Yoon, S. B. Kim, S. J. Yoo, and S. Ryu, “Ballast water treatment test at pilot-scale using an underwater capillary discharge device,” *Plasma Chemistry and Plasma Processing* **37**, 1405–1416 (2017).

- ³⁴G. Trenchev and A. Bogaerts, “Dual-vortex plasmatron: A novel plasma source for CO₂ conversion,” *Journal of CO₂ Utilization* **39**, 101152 (2020).
- ³⁵Y. Sui, C. A. Zorman, and R. M. Sankaran, “Plasmas for additive manufacturing,” *Plasma Processes and Polymers* **17**, 2000009 (2020).
- ³⁶P. J. Bruggeman, M. J. Kushner, B. R. Locke, J. G. Gardeniers, W. Graham, D. B. Graves, R. Hofman-Caris, D. Maric, J. P. Reid, E. Ceriani, *et al.*, “Plasma–liquid interactions: a review and roadmap,” *Plasma sources science and technology* **25**, 053002 (2016).
- ³⁷G. S. Oehrlein, R. J. Phaneuf, and D. B. Graves, “Plasma-polymer interactions: A review of progress in understanding polymer resist mask durability during plasma etching for nanoscale fabrication,” *Journal of Vacuum Science & Technology B* **29** (2011).
- ³⁸K. Becker, K. Schoenbach, and J. Eden, “Microplasmas and applications,” *Journal of Physics D: Applied Physics* **39**, R55 (2006).
- ³⁹Y. Kusano, “Atmospheric pressure plasma processing for polymer adhesion: A review,” *The Journal of Adhesion* **90**, 755–777 (2014).
- ⁴⁰J. Amorim, G. Baravian, and J. Jolly, “Laser-induced resonance fluorescence as a diagnostic technique in non-thermal equilibrium plasmas,” *Journal of Physics D: Applied Physics* **33**, R51 (2000).
- ⁴¹H. Döbele, T. Mosbach, K. Niemi, and V. Schulz-Von Der Gathen, “Laser-induced fluorescence measurements of absolute atomic densities: concepts and limitations,” *Plasma Sources Science and Technology* **14**, S31 (2005).
- ⁴²V. Donnelly, D. Flamm, and G. Collins, “Laser diagnostics of plasma etching: Measurement of Cl₂⁺ in a chlorine discharge,” *Journal of Vacuum Science and Technology* **21**, 817–823 (1982).
- ⁴³K. Konthasinghe, K. Fitzmorris, M. Peiris, A. J. Hopkins, B. Petrak, D. K. Killinger, and A. Muller, “Laser-induced fluorescence from N₂⁺ ions generated by a corona discharge in ambient air,” *Applied Spectroscopy* **69**, 1042–1046 (2015).
- ⁴⁴D. Lee, N. Hershkowitz, and G. D. Severn, “Measurements of Ar⁺ and Xe⁺ velocities near the sheath boundary of Ar–Xe plasma using two diode lasers,” *Applied Physics Letters* **91** (2007).
- ⁴⁵K. Tachibana, T. M. T. Mukai, and H. H. H. Harima, “Measurement of absolute densities and spatial distributions of Si and SiH in an RF-discharge silane plasma for the chemical vapor deposition of a-Si:H films,” *Japanese journal of applied physics* **30**, L1208 (1991).
- ⁴⁶G. Herring, M. J. Dyer, L. E. Jusinski, and W. K. Bischel, “Two-photon-excited fluorescence spectroscopy of atomic fluorine at 170 nm,” *Optics letters* **13**, 360–362 (1988).
- ⁴⁷G. S. Selwyn, L. Baston, and H. Sawin, “Detection of Cl and chlorine-containing negative ions in RF plasmas by two-photon laser-induced fluorescence,” *Applied physics letters* **51**, 898–900 (1987).
- ⁴⁸P. van de Weijer and B. H. Zwerfer, “Laser-induced fluorescence of OH and SiO molecules during thermal chemical vapour deposition of SiO₂ from silane-oxygen mixtures,” *Chemical physics letters* **163**, 48–54 (1989).

- ⁴⁹A. Diallo, S. Keller, Y. Shi, Y. Raitses, and S. Mazouffre, “Time-resolved ion velocity distribution in a cylindrical hall thruster: Heterodyne-based experiment and modeling,” *Review of Scientific Instruments* **86** (2015).
- ⁵⁰P. J. Bruggeman, N. Sadeghi, D. Schram, and V. Linss, “Gas temperature determination from rotational lines in non-equilibrium plasmas: a review,” *Plasma Sources Science and Technology* **23**, 023001 (2014).
- ⁵¹S. Yatom, N. Chopra, S. Kondeti, T. B. Petrova, Y. Raitses, D. R. Boris, M. J. Johnson, and S. G. Walton, “Measurement and reduction of Ar metastable densities by nitrogen admixing in electron beam-generated plasmas,” *Plasma Sources Science and Technology* **32**, 115005 (2023).
- ⁵²R. Forster, M. Frost, D. Fulle, H. Hamann, H. Hippler, A. Schlegel, and J. Troe, “High pressure range of the addition of HO to HO, NO, NO₂, and CO. I. Saturated laser induced fluorescence measurements at 298 K,” *The Journal of chemical physics* **103**, 2949–2958 (1995).
- ⁵³M. Mrkvičková, P. Dvořák, M. Svoboda, J. Kratzer, J. Voráč, and J. Dědina, “Dealing with saturation of the laser-induced fluorescence signal: An application to lead atoms,” *Combustion and Flame* **241**, 112100 (2022).
- ⁵⁴M. Goeckner, J. Goree, and T. Sheridan, “Saturation broadening of laser-induced fluorescence from plasma ions,” *Review of scientific instruments* **64**, 996–1000 (1993).
- ⁵⁵S. Mazouffre, “Laser-induced fluorescence spectroscopy applied to electric thrusters,” *Electric Propulsion Systems: from Recent Research Developments to Industrial Space Applications—STO-AVT* **263**, 1–10 (2016).
- ⁵⁶V. Kondeti, Y. Zheng, P. Luan, G. S. Oehrlein, and P. J. Bruggeman, “O, H, and OH radical etching probability of polystyrene obtained for a radio frequency driven atmospheric pressure plasma jet,” *Journal of Vacuum Science & Technology A* **38** (2020).
- ⁵⁷S. Yatom, Y. Luo, Q. Xiong, and P. J. Bruggeman, “Nanosecond pulsed humid Ar plasma jet in air: shielding, discharge characteristics and atomic hydrogen production,” *Journal of Physics D: Applied Physics* **50**, 415204 (2017).
- ⁵⁸V. Kondeti, U. Gangal, S. Yatom, and P. J. Bruggeman, “Ag⁺ reduction and silver nanoparticle synthesis at the plasma–liquid interface by an RF driven atmospheric pressure plasma jet: Mechanisms and the effect of surfactant,” *Journal of Vacuum Science & Technology A* **35** (2017).
- ⁵⁹P. Svarnas, I. Romadanov, A. Diallo, and Y. Raitses, “Laser-induced fluorescence of Xe I and Xe II in ambipolar plasma flow,” *IEEE Transactions on Plasma Science* **46**, 3998–4009 (2018).
- ⁶⁰L. Pietzonka, C. Eichhorn, F. Scholze, and D. Spemann, “Laser-induced fluorescence spectroscopy for kinetic temperature measurement of xenon neutrals and ions in the discharge chamber of a radiofrequency ion source,” *Journal of Electric Propulsion* **2**, 4 (2023).
- ⁶¹A. E. Vinci, S. Mazouffre, V. Gómez, P. Fajardo, and J. Navarro-Cavallé, “Laser-induced fluorescence spectroscopy on xenon atoms and ions in the magnetic nozzle of a helicon plasma thruster,” *Plasma Sources Science and Technology* **31**, 095007 (2022).

- ⁶²C. Brackmann, B. Zhou, Z. Li, and M. Alden, “Strategies for quantitative planar laser-induced fluorescence of NH radicals in flames,” *Combustion Science and Technology* **188**, 529–541 (2016).
- ⁶³A. Hirano and M. Tsujishita, “Visualization of CN by the use of planar laser-induced fluorescence in a cross section of an unseeded turbulent CH₄–air flame,” *Applied optics* **33**, 7777–7780 (1994).
- ⁶⁴B. J. Kirby and B. K. Hanson, “Imaging of CO and CO₂ using infrared planar laser-induced fluorescence,” *Proceedings of the Combustion Institute* **28**, 253–259 (2000).
- ⁶⁵A. D. Sappey and T. K. Gamble, “Planar laser-induced fluorescence imaging of Cu atom and Cu₂ in a condensing laser-ablated copper plasma plume,” *Journal of applied physics* **72**, 5095–5107 (1992).
- ⁶⁶K. Niemi, V. Schulz-Von Der Gathen, and H. Döbele, “Absolute calibration of atomic density measurements by laser-induced fluorescence spectroscopy with two-photon excitation,” *Journal of Physics D: Applied Physics* **34**, 2330 (2001).
- ⁶⁷W. D. Kulatilaka, J. H. Frank, and T. B. Settersten, “Interference-free two-photon LIF imaging of atomic hydrogen in flames using picosecond excitation,” *Proceedings of the Combustion Institute* **32**, 955–962 (2009).
- ⁶⁸A. Dogariu, E. Evans, S. P. Vinoth, and S. A. Cohen, “Non-invasive neutral atom density measurements using fs-TALIF in a magnetic linear plasma device,” in *CLEO: Science and Innovations* (Optica Publishing Group, 2021) pp. SM1E–1.
- ⁶⁹S. Yatom and D. Dobrynin, “Examination of OH and H₂O₂ production by uniform and non-uniform modes of dielectric barrier discharge in He/air mixture,” *Journal of Physics D: Applied Physics* **55**, 485203 (2022).
- ⁷⁰F. Träger, *Springer handbook of lasers and optics*, Vol. 2 (Springer, 2012).
- ⁷¹K. F. Renk, *Basics of laser physics* (Springer, 2012).
- ⁷²V. Vekselman, J. Gleizer, S. Yatom, V. T. Gurovich, and Y. E. Krasik, “High-current diode with ferroelectric plasma source-assisted hollow anode,” *Journal of Applied Physics* **108** (2010).
- ⁷³T. Verreycken, R. Mensink, R. Van Der Horst, N. Sadeghi, and P. J. Bruggeman, “Absolute OH density measurements in the effluent of a cold atmospheric-pressure Ar–H₂O RF plasma jet in air,” *Plasma Sources Science and Technology* **22**, 055014 (2013).
- ⁷⁴R. B. Miles, W. R. Lempert, and J. N. Forkey, “Laser Rayleigh scattering,” *Measurement Science and Technology* **12**, R33 (2001).
- ⁷⁵W. Kauzmann, *Kinetic theory of gases* (Courier Corporation, 2012).
- ⁷⁶G. J. Fiechtner and J. R. Gord, “Absorption and the dimensionless overlap integral for two-photon excitation,” *Journal of Quantitative Spectroscopy and Radiative Transfer* **68**, 543–557 (2001).
- ⁷⁷J. Luque and D. Crosley, “Absolute CH concentrations in low-pressure flames measured with laser-induced fluorescence,” *Applied Physics B* **63**, 91–98 (1996).
- ⁷⁸S. Nemschokmichal and J. Meichsner, “N₂(A³Σ_u⁺) metastable density in nitrogen barrier discharges: I. LIF diagnostics and absolute calibration by Rayleigh scattering,” *Plasma Sources Science and Technology* **22**, 015005 (2012).

- ⁷⁹A. Kramida, Yu. Ralchenko, J. Reader, and NIST ASD Team, NIST Atomic Spectra Database (ver. 5.11), [Online]. Available: <https://physics.nist.gov/asd> [2024, June 1]. National Institute of Standards and Technology, Gaithersburg, MD. (2024).
- ⁸⁰K. Huber, *Molecular spectra and molecular structure: IV. Constants of diatomic molecules* (Springer Science & Business Media, 2013).
- ⁸¹C. Kaminski and P. Ewart, “Absolute concentration measurements of C₂ in a diamond CVD reactor by laser-induced fluorescence,” *Applied Physics B* **61**, 585–592 (1995).
- ⁸²J. Luque, W. Juchmann, and J. Jeffries, “Spatial density distributions of C₂, C₃, and CH radicals by laser-induced fluorescence in a diamond depositing DC-arcjet,” *Journal of applied physics* **82**, 2072–2081 (1997).
- ⁸³J. B. Schmidt, *Ultrashort Two-Photon-Absorption Laser-Induced Fluorescence in Nanosecond-Duration, Repetitively Pulsed Discharges*, Ph.D. thesis, The Ohio State University (2015).
- ⁸⁴R. Stern and J. Johnson III, “Plasma ion diagnostics using resonant fluorescence,” *Physical Review Letters* **34**, 1548 (1975).
- ⁸⁵V. Vekselman, J. Gleizer, S. Yatom, D. Yarmolich, V. T. Gurovich, G. Bazalitski, Y. E. Krasik, and V. Bernshtam, “Laser induced fluorescence of the ferroelectric plasma source assisted hollow anode discharge,” *Physics of Plasmas* **16** (2009).
- ⁸⁶V. Gavrilenko, H. Kim, T. Ikutake, J. Kim, Y. Choi, M. Bowden, and K. Muraoka, “Measurement method for electric fields based on stark spectroscopy of argon atoms,” *Physical Review E* **62**, 7201 (2000).
- ⁸⁷B. B. Ngom, T. B. Smith, W. Huang, and A. D. Gallimore, “Numerical simulation of the zeeman effect in neutral xenon from nir diode-laser spectroscopy,” *Journal of Applied Physics* **104** (2008).
- ⁸⁸J. Pérez-Luna, G. J. M. Hagelaar, L. Garrigues, and J. P. Boeuf, “Method to obtain the electric field and the ionization frequency from laser induced fluorescence measurements,” *Plasma Sources Science and Technology* **18**, 034008 (2009).
- ⁸⁹C. Cohen-Tannoudji, B. Diu, and F. Laloë, *Quantum Mechanics Volume 1* (Hermann, 1977).
- ⁹⁰I. Romadanov, Y. Raitses, A. Diallo, K. Hara, I. Kaganovich, and A. Smolyakov, “On limitations of laser-induced fluorescence diagnostics for xenon ion velocity distribution function measurements in hall thrusters,” *Physics of Plasmas* **25** (2018).
- ⁹¹S. Mazouffre, “Laser-induced fluorescence diagnostics of the cross-field discharge of hall thrusters,” *Plasma Sources Science and Technology* **22**, 013001 (2012).
- ⁹²V. Chaplin, R. Lobbia, A. Lopez Ortega, I. Mikellides, R. Hofer, J. Polk, and A. Friss, “Time-resolved ion velocity measurements in a high-power hall thruster using laser-induced fluorescence with transfer function averaging,” *Applied Physics Letters* **116** (2020).
- ⁹³J. Vaudolon, B. Khiar, and S. Mazouffre, “Time evolution of the electric field in a hall thruster,” *Plasma Sources Science and Technology* **23**, 022002 (2014).
- ⁹⁴C. V. Young, A. L. Fabris, N. A. MacDonald-Tenenbaum, W. A. Hargus, and M. A. Cappelli, “Time-resolved laser-induced fluorescence diagnostics for electric propulsion and their application to breathing mode dynamics,” *Plasma Sources Science and Technology* **27**, 094004 (2018).

- ⁹⁵M. Aramaki, K. Ogiwara, S. Etoh, S. Yoshimura, and M. Y. Tanaka, “High resolution laser induced fluorescence Doppler velocimetry utilizing saturated absorption spectroscopy,” *Review of Scientific Instruments* **80** (2009).
- ⁹⁶R. Boivin and E. Scime, “Laser induced fluorescence in Ar and He plasmas with a tunable diode laser,” *Review of scientific instruments* **74**, 4352–4360 (2003).
- ⁹⁷W. Huang, T. Smith, and A. Gallimore, “Obtaining velocity distribution using a xenon ion line with unknown hyperfine constants,” in *40th AIAA Plasmadynamics and Lasers Conference* (2009) p. 4226.
- ⁹⁸H.-J. Kunze, *Introduction to plasma spectroscopy*, Vol. 56 (Springer Science & Business Media, 2009).
- ⁹⁹S. Hübner, N. Sadeghi, E. Carbone, and J. Van Der Mullen, “Density of atoms in ar*(3p54s) states and gas temperatures in an argon surfatron plasma measured by tunable laser spectroscopy,” *Journal of Applied Physics* **113** (2013).
- ¹⁰⁰E. Scime, C. Biloiu, C. Compton, F. Doss, D. Venture, J. Heard, E. Choueiri, and R. Spektor, “Laser induced fluorescence in a pulsed argon plasma,” *Review of Scientific Instruments* **76** (2005).
- ¹⁰¹B. Pelissier and N. Sadeghi, “Time-resolved pulse-counting lock-in detection of laser induced fluorescence in the presence of a strong background emission,” *Review of scientific instruments* **67**, 3405–3410 (1996).
- ¹⁰²J. Vaudolon, L. Balika, and S. Mazouffre, “Photon counting technique applied to time-resolved laser-induced fluorescence measurements on a stabilized discharge,” *Review of Scientific Instruments* **84** (2013).
- ¹⁰³B. Jacobs, W. Gekelman, P. Pribyl, M. Barnes, and M. Kilgore, “Laser-induced fluorescence measurements in an inductively coupled plasma reactor,” *Applied Physics Letters* **91** (2007).
- ¹⁰⁴I. Romadanov, Y. Raitses, and A. Smolyakov, “Wavelength modulation laser-induced fluorescence for plasma characterization,” arXiv preprint arXiv:2403.11045 (2024).
- ¹⁰⁵L. Dixit and S. Ram, “Quantitative analysis by derivative electronic spectroscopy,” *Applied Spectroscopy Reviews* **21**, 311–418 (1985).
- ¹⁰⁶W. Amos and J. White, “How the confocal laser scanning microscope entered biological research,” *Biology of the Cell* **95**, 335–342 (2003).
- ¹⁰⁷R. VanDervort, D. Elliott, D. McCarren, J. McKee, M. Soderholm, S. Sears, and E. Scime, “Optimization of confocal laser induced fluorescence in a plasma,” *Review of Scientific Instruments* **85** (2014).
- ¹⁰⁸D. S. Thompson, M. F. Henriquez, E. E. Scime, and T. N. Good, “Confocal laser induced fluorescence with comparable spatial localization to the conventional method,” *Review of Scientific Instruments* **88** (2017).
- ¹⁰⁹T. Kajiwara, K. Takeda, K. Muraoka, T. Okada, M. Maeda, and M. Akazaki, “Coaxial laser fluorescence system by two-photon excitation for atomic hydrogen detection in high-temperature plasmas,” *Japanese Journal of Applied Physics* **29**, L826 (1990).
- ¹¹⁰D. Caron, R. John, E. Scime, and T. Steinberger, “Ion velocity distribution functions across a plasma meniscus,” *Journal of Vacuum Science & Technology A* **41** (2023).

- ¹¹¹I. Romadanov and Y. Raitses, “A confocal laser-induced fluorescence diagnostic with an annular laser beam,” *Review of Scientific Instruments* **94** (2023).
- ¹¹²J. Lee, A. Efremov, and K.-H. Kwon, “On the relationships between plasma chemistry, etching kinetics and etching residues in $\text{CF}_4 + \text{C}_4\text{F}_8 + \text{Ar}$ and $\text{CF}_4 + \text{CH}_2\text{F}_2 + \text{Ar}$ plasmas with various $\text{CF}_4/\text{C}_4\text{F}_8$ and $\text{CF}_4/\text{CH}_2\text{F}_2$ mixing ratios,” *Vacuum* **148**, 214–223 (2018).
- ¹¹³M. Foad, C. Wilkinson, C. Dunscomb, and R. Williams, “ CH_4/H_2 : A universal reactive ion etch for II-VI semiconductors?” *Applied physics letters* **60**, 2531–2533 (1992).
- ¹¹⁴F. Bell, O. Joubert, G. Oehrlein, Y. Zhang, and D. Vender, “Investigation of selective SiO_2 -to-Si etching in an inductively coupled high-density plasma using fluorocarbon gases,” *Journal of Vacuum Science & Technology A: Vacuum, Surfaces, and Films* **12**, 3095–3101 (1994).
- ¹¹⁵X. Li, X. Hua, L. Ling, G. S. Oehrlein, M. Barela, and H. M. Anderson, “Fluorocarbon-based plasma etching of SiO_2 : Comparison of $\text{C}_4\text{F}_6/\text{Ar}$ and $\text{C}_4\text{F}_8/\text{Ar}$ discharges,” *Journal of Vacuum Science & Technology A: Vacuum, Surfaces, and Films* **20**, 2052–2061 (2002).
- ¹¹⁶S.-W. Cho, C.-K. Kim, J.-K. Lee, S. H. Moon, and H. Chae, “Angular dependences of SiO_2 etch rates in $\text{C}_4\text{F}_6/\text{O}_2/\text{Ar}$ and $\text{C}_4\text{F}_6/\text{CH}_2\text{F}_2/\text{O}_2/\text{Ar}$ plasmas,” *Journal of Vacuum Science & Technology A* **30** (2012).
- ¹¹⁷H. Rhee, H. Kwon, C.-K. Kim, H. Kim, J. Yoo, and Y. W. Kim, “Comparison of deep silicon etching using $\text{SF}_6/\text{C}_4\text{F}_8$ and $\text{SF}_6/\text{C}_4\text{F}_6$ plasmas in the bosch process,” *Journal of Vacuum Science & Technology B: Microelectronics and Nanometer Structures Processing, Measurement, and Phenomena* **26**, 576–581 (2008).
- ¹¹⁸R. d’Agostino and D. L. Flamm, “Plasma etching of Si and SiO_2 in $\text{SF}_6\text{--O}_2$ mixtures,” *Journal of Applied Physics* **52**, 162–167 (1981).
- ¹¹⁹A. Efremov, V. Betelin, and K.-H. Kwon, “Kinetics and mechanisms of reactive-ion etching of Si and SiO_2 in a plasma of a mixture of $\text{HBr} + \text{O}_2$,” *Russian Microelectronics* **49**, 379–384 (2020).
- ¹²⁰J. K. Kim, S. I. Cho, N. G. Kim, M. S. Jhon, K. S. Min, C. K. Kim, and G. Y. Yeom, “Study on the etching characteristics of amorphous carbon layer in oxygen plasma with carbonyl sulfide,” *Journal of Vacuum Science & Technology A* **31** (2013).
- ¹²¹L. Jiang, N. Plank, M. Blauw, R. Cheung, and E. van der Drift, “Dry etching of SiC in inductively coupled Cl_2/Ar plasma,” *Journal of Physics D: Applied Physics* **37**, 1809 (2004).
- ¹²²V. M. Donnelly, D. L. Flamm, W. Dautremont-Smith, and D. Werder, “Anisotropic etching of SiO_2 in low-frequency CF_4/O_2 and NF_3/Ar plasmas,” *Journal of applied physics* **55**, 242–252 (1984).
- ¹²³H. Nishino, N. Hayasaka, and H. Okano, “Damage-free selective etching of Si native oxides using NH_3/NF_3 and $\text{SF}_6/\text{H}_2\text{O}$ down-flow etching,” *Journal of applied physics* **74**, 1345–1348 (1993).
- ¹²⁴M. M. Hefny, C. Pattyn, P. Lukes, and J. Benedikt, “Atmospheric plasma generates oxygen atoms as oxidizing species in aqueous solutions,” *Journal of Physics D: Applied Physics* **49**, 404002 (2016).
- ¹²⁵S. Yatom, “Diagnostics of plasma–liquids systems: Challenges and their mitigation,” *Physics of Plasmas* **30** (2023).

- ¹²⁶A. Colibaba-Evulet, A. Singhal, and N. Glumac, "Detection of AlO and TiO by laser-induced fluorescence in powder synthesis flames," *Combustion science and technology* **157**, 129–139 (2000).
- ¹²⁷K. Honma, "Reaction dynamics of $\text{Al} + \text{O}_2 \rightarrow \text{AlO} + \text{O}$ studied by the crossed-beam laser-induced fluorescence technique," *The Journal of chemical physics* **119**, 3641–3649 (2003).
- ¹²⁸J. Li, M. Xu, X. Li, Q. Ma, N. Zhao, Q. Zhang, L. Guo, and Y. Lu, "Laser-induced molecular fluorescence diagnosis of aluminum monoxide evolution in laser-induced plasma," *Laser Physics Letters* **16**, 055701 (2019).
- ¹²⁹M. He, H. Wang, and B. R. Weiner, "Production and laser-induced fluorescence spectrum of aluminum sulfide," *Chemical physics letters* **204**, 563–566 (1993).
- ¹³⁰A. L. Alstrin, R. V. Smilgys, P. G. Strupp, and S. R. Leone, "Vibrational distributions of As_2 in the cracking of As_4 on Si (100) and Si (111)," *The Journal of chemical physics* **97**, 6864–6870 (1992).
- ¹³¹V. Donnelly and R. Karlicek, "Development of laser diagnostic probes for chemical vapor deposition of InP/InGaAsP epitaxial layers," *Journal of Applied Physics* **53**, 6399–6407 (1982).
- ¹³²R. V. Smilgys and S. R. Leone, "State-resolved laser probing of As_2 in a molecular-beam epitaxy reactor," *Journal of Vacuum Science & Technology B: Microelectronics Processing and Phenomena* **8**, 416–421 (1990).
- ¹³³Y. Ng, H. Pang, and A.-C. Cheung, "Laser induced fluorescence spectroscopy of boron carbide," *Chemical Physics Letters* **509**, 16–19 (2011).
- ¹³⁴F. X. Sunahori, R. Nagarajan, and D. J. Clouthier, "Optical-optical double resonance, laser induced fluorescence, and revision of the signs of the spin-spin constants of the boron carbide (BC) free radical," *The Journal of Chemical Physics* **143** (2015).
- ¹³⁵C. Fleddermann and G. Hebner, "Measurements of relative BCl density in BCl_3 -containing inductively coupled radio frequency plasmas," *Journal of applied physics* **83**, 4030–4036 (1998).
- ¹³⁶J. Rice, N. Caldwell, and H. Nelson, "Gas-phase reaction kinetics of boron monohydride," *The Journal of Physical Chemistry* **93**, 3600–3605 (1989).
- ¹³⁷J. Harrison, R. Meads, and L. Phillips, "Kinetics of reactions of BH with NO and C_2H_4 ," *Chemical physics letters* **150**, 299–302 (1988).
- ¹³⁸F. X. Sunahori, M. Gharaibeh, D. J. Clouthier, and R. Tarroni, "BH₂ revisited: New, extensive measurements of laser-induced fluorescence transitions and ab initio calculations of near-spectroscopic accuracy," *The Journal of Chemical Physics* **142** (2015).
- ¹³⁹M. A. Clyne and M. C. Heaven, "Laser-induced fluorescence of the BO and BO_2 free radicals," *Chemical Physics* **51**, 299–309 (1980).
- ¹⁴⁰P. Maksyutenko, D. S. Parker, F. Zhang, and R. I. Kaiser, "An LIF characterization of supersonic BO ($X^2\Sigma^+$) and CN ($X^2\Sigma^+$) radical sources for crossed beam studies," *Review of Scientific Instruments* **82** (2011).

- ¹⁴¹G. R. Schneider and W. B. Roh, "Application of laser-induced fluorescence in an atmospheric-pressure boron-seeded flame," AIP Conference Proceedings **172**, 753–755 (1988).
- ¹⁴²K. Weyer, R. Beaudet, R. Straubinger, and H. Walther, "Laser excited fluorescence of the II vibronic states of BO₂," Chemical Physics **47**, 171–178 (1980).
- ¹⁴³S.-G. He, C. J. Evans, and D. J. Clouthier, "A study of the molecular structure and Renner–Teller effect in the $\tilde{A}^2\Pi_u - \tilde{X}^2\Pi_g$ electronic spectrum of jet-cooled boron disulfide, BS₂," The Journal of chemical physics **119**, 2047–2056 (2003).
- ¹⁴⁴C. Focsa, H. Li, and P. Bernath, "Characterization of the Ground State of Br₂ by Laser-Induced Fluorescence Fourier Transform Spectroscopy of the B³ $\Pi_{0+u} - X^1\Sigma_g^+$ System," Journal of Molecular Spectroscopy **200**, 104–119 (2000).
- ¹⁴⁵S. Bullman, J. Farthing, and J. Whitehead, "Laser-induced fluorescence studies of a supersonic molecular beam of bromine: Vibrational and rotational relaxation of bromine and collision-free lifetimes for Br₂ (B₃ $\Pi(0_u^+)$)," Molecular Physics **44**, 97–109 (1981).
- ¹⁴⁶M. Nakajima, T. W. Schmidt, Y. Sumiyoshi, and Y. Endo, "Rotationally-resolved excitation spectrum of the jet-cooled cyclohexadienyl radical," Chemical Physics Letters **449**, 57–62 (2007).
- ¹⁴⁷S. Zhou, M. Zhan, J. Shi, and C. Wang, "Gas phase spectrum of dibromocarbene studied by laser-induced fluorescence," Chemical physics letters **166**, 547–550 (1990).
- ¹⁴⁸C.-L. Lee, M.-L. Liu, and B.-C. Chang, "Electronic spectroscopy of bromomethylenes in a supersonic free jet expansion," Physical Chemistry Chemical Physics **5**, 3859–3863 (2003).
- ¹⁴⁹W. Hack, "Detection methods for atoms and radicals in the gas phase," International Reviews in Physical Chemistry **4**, 165–200 (1985).
- ¹⁵⁰J. Tiee, F. Wampler, and W. Rice Jr, "Reactions of CCl, CCl₂ and CClF radicals," Chemical Physics Letters **73**, 519–521 (1980).
- ¹⁵¹R. Huie, N. Long, and B. Thrush, "Laser induced fluorescence of CFCl and CCl₂ in the gas phase," Chemical Physics Letters **51**, 197–200 (1977).
- ¹⁵²N. D. Gómez, V. D'accurso, V. M. Freytes, F. A. Manzano, J. Codnia, and M. L. Azcárate, "Kinetic Study of the CCl₂ Radical Recombination Reaction by Laser-Induced Fluorescence Technique," International Journal of Chemical Kinetics **45**, 306–313 (2013).
- ¹⁵³Y. Liu, Y. Xin, L. Pei, Y. Chen, and C. Chen, "Reaction kinetic studies of CCl₂ (X (0, 0, 0)) with several simple molecules," Chemical physics letters **385**, 314–318 (2004).
- ¹⁵⁴Q. Lu, Y. Chen, D. Wang, Y. Zhang, S. Yu, C. Chen, M. Koshi, H. Matsui, S. Koda, and X. Ma, "Laser-induced fluorescence excitation spectrum of CCl₂ cooled in a supersonic free jet," Chemical physics letters **178**, 517–522 (1991).
- ¹⁵⁵J. Tiee, F. Wampler, and W. Rice, "Laser-induced fluorescence excitation spectra of CCl₂ and CFCI radicals in the gas phase," Chemical Physics Letters **65**, 425–428 (1979).

- ¹⁵⁶J. S. Guss, C. A. Richmond, K. Nauta, and S. H. Kable, “Laser-induced fluorescence excitation and dispersed fluorescence spectroscopy of the $\tilde{A}(^1B_1) - \tilde{X}(^1A_1)$ transition of dichlorocarbene,” *Physical Chemistry Chemical Physics* **7**, 100–108 (2005).
- ¹⁵⁷M. Ludwiczak, D. Latimer, and R. Steer, “The $\tilde{B} - \tilde{X}$ laser-induced fluorescence excitation spectrum of jet-cooled Cl_2CS : Origin location and partial vibronic analysis,” *Journal of Molecular Spectroscopy* **147**, 414–430 (1991).
- ¹⁵⁸J. Booth, G. Hancock, N. Perry, and M. Toogood, “Spatially and temporally resolved laser-induced fluorescence measurements of CF_2 and CF radicals in a CF_4 RF plasma,” *Journal of applied physics* **66**, 5251–5257 (1989).
- ¹⁵⁹D. S. King, P. K. Schenck, and J. C. Stephenson, “Spectroscopy and photophysics of the $CF_2 \tilde{A}^1B_1 - \tilde{X}^1A_1$ system,” *Journal of Molecular Spectroscopy* **78**, 1–15 (1979).
- ¹⁶⁰B. K. McMillin and M. R. Zachariah, “Two-dimensional imaging of CF_2 density by laser-induced fluorescence in CF_4 etching plasmas in the gaseous electronics conference reference cell,” *Journal of Vacuum Science & Technology A: Vacuum, Surfaces, and Films* **15**, 230–237 (1997).
- ¹⁶¹L. Rubio, M. Santos, and J. Torresano, “Laser induced fluorescence detection of CF , CF_2 and CF_3 in the infrared multiphoton dissociation of C_3F_6 ,” *Journal of Photochemistry and Photobiology A: Chemistry* **146**, 1–8 (2001).
- ¹⁶²M.-C. Yang, J. Williamson, and T. A. Miller, “Rotational analyses of the laser induced fluorescence excitation spectra of jet-cooled CF_3O and CF_3S ,” *Journal of molecular spectroscopy* **186**, 1–14 (1997).
- ¹⁶³Z. Li and J. Francisco, “Laser-induced fluorescence spectroscopic study of the $\tilde{A}^2A_1 - \tilde{X}^2E$ transition of trifluoromethoxy radical,” *Chemical physics letters* **186**, 336–342 (1991).
- ¹⁶⁴J. Purdy and B. Thrush, “Laser-induced fluorescence of $CFBr$ in the gas phase,” *Chemical Physics Letters* **73**, 228–230 (1980).
- ¹⁶⁵B. S. Truscott, N. L. Elliott, and C. M. Western, “A reanalysis of the $\tilde{A}^1A'' - \tilde{X}''A''$ transition of $CFBr$,” *The Journal of chemical physics* **130** (2009).
- ¹⁶⁶J. S. Guss, O. Votava, and S. H. Kable, “Electronic spectroscopy of jet-cooled $CFCl$: Laser-induced fluorescence, dispersed fluorescence, lifetimes, and $C-Cl$ dissociation barrier,” *The Journal of Chemical Physics* **115**, 11118–11130 (2001).
- ¹⁶⁷G. A. Raiche and J. B. Jeffries, “Laser-induced fluorescence temperature measurements in a dc arcjet used for diamond deposition,” *Applied optics* **32**, 4629–4635 (1993).
- ¹⁶⁸J. Luque, W. Juchmann, and J. Jeffries, “Absolute concentration measurements of CH radicals in a diamond-depositing dc-arcjet reactor,” *Applied optics* **36**, 3261–3270 (1997).
- ¹⁶⁹M. Engelhard, W. Jacob, W. Möller, and A. Koch, “New calibration method for the determination of the absolute density of CH radicals through laser-induced fluorescence,” *Applied optics* **34**, 4542–4551 (1995).
- ¹⁷⁰J. Luque, R. Klein-Douwel, J. Jeffries, G. Smith, and D. Crosley, “Quantitative laser-induced fluorescence of CH in atmospheric pressure flames,” *Applied Physics B* **75**, 779–790 (2002).

- ¹⁷¹K. Hakuta, "Vibration-rotation spectrum of HCF (X^1A') by laser-induced fluorescence," *Journal of Molecular Spectroscopy* **106**, 56–63 (1984).
- ¹⁷²D. L'Espérance, B. A. Williams, and J. W. Fleming, "Detection of fluorocarbon intermediates in low-pressure premixed flames by laser-induced fluorescence," *Chemical physics letters* **280**, 113–118 (1997).
- ¹⁷³M. Kakimoto, S. Saito, and E. Hirota, "Doppler-limited dye laser excitation spectroscopy of HCF," *Journal of Molecular Spectroscopy* **88**, 300–310 (1981).
- ¹⁷⁴Y. Qiu, S. Zhou, and J. Shi, "Laser-induced fluorescence of HCF and HCCl," *Chemical physics letters* **136**, 93–96 (1987).
- ¹⁷⁵M. N. Ashfold, F. Castano, G. Hancock, and G. Ketley, "Laser-induced fluorescence of the CHF radical," *Chemical Physics Letters* **73**, 421–424 (1980).
- ¹⁷⁶G. Hancock and G. W. Ketley, "CHF (X^1A') radical kinetics. Part 1.—Reaction with NO and O₂," *Journal of the Chemical Society, Faraday Transactions 2: Molecular and Chemical Physics* **78**, 1283–1291 (1982).
- ¹⁷⁷T. W. Schmidt, G. B. Bacskay, and S. H. Kable, "Characterization of the $\tilde{A}(^1A'')$ state of HCF by laser induced fluorescence spectroscopy," *The Journal of chemical physics* **110**, 11277–11285 (1999).
- ¹⁷⁸J. Danon, S. Filseth, D. Feldmann, H. Zacharias, C. Dugan, and K. Welge, "Laser induced fluorescence of CH₂ (\tilde{a}^1A_1) produced in the photodissociation of ketene at 337 nm. The CH₂ (\tilde{a}^1A_1 - \tilde{X}^3B_1) energy separation," *Chemical Physics* **29**, 345–351 (1978).
- ¹⁷⁹C. Brackmann, Z. Li, M. Rupinski, N. Docquier, G. Pengloan, and M. Aldén, "Strategies for formaldehyde detection in flames and engines using a single-mode Nd: YAG/OPO laser system," *Applied spectroscopy* **59**, 763–768 (2005).
- ¹⁸⁰J. E. Harrington and K. C. Smyth, "Laser-induced fluorescence measurements of formaldehyde in a methane/air diffusion flame," *Chemical Physics Letters* **202**, 196–202 (1993).
- ¹⁸¹D. Gutman, N. Sanders, and J. Butler, "Kinetics of the reactions of methoxy and ethoxy radicals with oxygen," *The Journal of Physical Chemistry* **86**, 66–70 (1982).
- ¹⁸²T. Ebata, H. Yanagishita, K. Obi, and I. Tanaka, " $\tilde{A} \rightarrow \tilde{X}$ fluorescence spectra of CH₃O and C₂H₅O generated by the ArF laser photolysis of alkyl nitrites," *Chemical Physics* **69**, 27–33 (1982).
- ¹⁸³G. Inoue, H. Akimoto, and M. Okuda, "Laser-induced fluorescence spectra of CH₃O," *Chemical Physics Letters* **63**, 213–216 (1979).
- ¹⁸⁴G. Inoue, H. Akimoto, and M. Okuda, "Spectroscopy of the CH₃O A^2A_1 - X^2E system by laser-excited fluorescence method," *The Journal of Chemical Physics* **72**, 1769–1775 (1980).
- ¹⁸⁵J. Kappert and F. Temps, "Rotationally resolved laser-induced fluorescence excitation studies of CH₃O," *Chemical Physics* **132**, 197–208 (1989).
- ¹⁸⁶L. Zu, J. Liu, G. Tarczay, P. Dupré, and T. A. Miller, "Jet-cooled laser spectroscopy of the cyclohexoxy radical," *The Journal of chemical physics* **120**, 10579–10593 (2004).

- ¹⁸⁷M. Suzuki, G. Inoue, and H. Akimoto, "Laser induced fluorescence of CH₃S and CD₃S radicals," *The Journal of chemical physics* **81**, 5405–5412 (1984).
- ¹⁸⁸G. Black and L. E. Jusinski, "Laser-induced fluorescence studies of the CH₃S radical," *Journal of the Chemical Society, Faraday Transactions 2: Molecular and Chemical Physics* **82**, 2143–2151 (1986).
- ¹⁸⁹C. Conley, J. B. Halpern, J. Wood, C. Vaughn, and W. M. Jackson, "Laser excitation of the CN B²Σ⁺ ← A²Π 0–0 and 1–0 bands," *Chemical Physics Letters* **73**, 224–227 (1980).
- ¹⁹⁰R. Cody, M. J. Sabety-Dzvonik, and W. Jackson, "Laser-induced fluorescence of CN(X²Σ⁺) produced by photolysis of C₂N₂ at 160 nm," *The Journal of Chemical Physics* **66**, 2145–2152 (1977).
- ¹⁹¹P. Bonczyk and J. Shirley, "Measurement of CH and CN concentration in flames by laser-induced saturated fluorescence," *Combustion and flame* **34**, 253–264 (1979).
- ¹⁹²J. A. Sutton, B. A. Williams, and J. W. Fleming, "Laser-induced fluorescence measurements of NCN in low-pressure CH₄/O₂/N₂ flames and its role in prompt NO formation," *Combustion and Flame* **153**, 465–478 (2008).
- ¹⁹³G. P. Smith, R. A. Copeland, and D. R. Crosley, "Electronic quenching, fluorescence lifetime, and spectroscopy of the A³Π_u state of NCN," *The Journal of chemical physics* **91**, 1987–1993 (1989).
- ¹⁹⁴M. Curtis, A. Levick, and P. Sarre, "Laser-induced-fluorescence spectrum of the CNN molecule," *Laser chemistry* **9**, 359–368 (1988).
- ¹⁹⁵B. Dally, A. Masri, R. Barlow, and G. Fiechtner, "Two-photon laser-induced fluorescence measurement of CO in turbulent non-premixed bluff body flames," *Combustion and flame* **132**, 272–274 (2003).
- ¹⁹⁶J. Zetterberg, S. Blomberg, J. Gustafson, Z. Sun, Z. Li, E. Lundgren, and M. Aldén, "An in situ set up for the detection of CO₂ from catalytic CO oxidation by using planar laser-induced fluorescence," *Review of scientific instruments* **83** (2012).
- ¹⁹⁷Z. Alwahabi, J. Zetterberg, Z. Li, and M. Aldén, "High resolution polarization spectroscopy and laser induced fluorescence of CO₂ around 2μm," *The European Physical Journal D* **42**, 41–47 (2007).
- ¹⁹⁸P. Clough and J. Johnston, "Laser-induced fluorescence measurement of the vibrational distribution of CS formed in the reaction O+ CS₂ → CS + SO," *Chemical Physics Letters* **71**, 253–257 (1980).
- ¹⁹⁹A. J. Hynes and J. H. Brophy, "Laser-induced fluorescence study of radiative lifetimes and quenching rates in CS A¹Π (ν= 0)," *Chemical physics letters* **63**, 93–96 (1979).
- ²⁰⁰M. Martin and R. J. Donovan, "Two-photon dissociation of CS₂ with a KrF laser (λ= 248 nm)," *Journal of Photochemistry* **18**, 245–250 (1982).
- ²⁰¹N. Ochi, H. Watanabe, S. Tsuchiya, and S. Koda, "Rotationally resolved laser-induced fluorescence and zeeman quantum beat spectroscopy of the V ¹B₂ state of jet-cooled CS₂," *Chemical physics* **113**, 271–285 (1987).
- ²⁰²T. Weyh and W. Demtröder, "Lifetime measurements of selectively excited rovibrational levels of the V¹B₂ state of CS₂," *The Journal of chemical physics* **104**, 6938–6948 (1996).

- ²⁰³E. Martínez, M. López, J. Albaladejo, and F. Poblete, “Laser-induced fluorescence from selected excited states of the CS₂ molecule,” *Journal of molecular structure* **408**, 553–556 (1997).
- ²⁰⁴W. N. Sisk, N. Sarkar, S. Ikeda, and H. Hayashi, “Influence of large magnetic fields on fluorescence of gaseous CS₂ excited through several V bands,” *The Journal of Physical Chemistry A* **103**, 7179–7185 (1999).
- ²⁰⁵F. X. Sunahori, X. Zhang, and D. J. Clouthier, “The electronic spectrum of jet-cooled copper hydrosulfide (cush),” *The Journal of chemical physics* **125** (2006).
- ²⁰⁶R. Dreyfus, “Cu⁰, Cu⁺, and Cu₂ from excimer-ablated copper,” *Journal of applied physics* **69**, 1721–1729 (1991).
- ²⁰⁷V. Vekselman, A. Khrabry, I. Kaganovich, B. Stratton, R. Selinsky, and Y. Raites, “Quantitative imaging of carbon dimer precursor for nanomaterial synthesis in the carbon arc,” *Plasma Sources Science and Technology* **27**, 025008 (2018).
- ²⁰⁸H. Reisler, M. Mangir, and C. Wittig, “The kinetics of free radicals generated by IR laser photolysis. II. Reactions of C₂(X¹Σ_g⁺), C₂(a³Π_u), C₃($\tilde{X}^1\Sigma_g^+$) and CN(X²Σ⁺) with O₂,” *Chemical Physics* **47**, 49–58 (1980).
- ²⁰⁹W. M. Pitts, L. Pasternack, and J. McDonald, “Temperature dependence of the C₂(X¹Σ_g⁺) reaction with H₂ and CH₄ and C₂(X¹Σ_g⁺ and a³Π_u equilibrated states) with O₂,” *Chemical Physics* **68**, 417–422 (1982).
- ²¹⁰D. Jones and J. Mackie, “Evaluation of C₂ resonance fluorescence as a technique for transient flame studies,” *Combustion and Flame* **27**, 143–146 (1976).
- ²¹¹T. Tatarczyk, E. Fink, and K. Becker, “Lifetime measurements on single vibrational levels of C₂(d³Π_g) by laser fluorescence excitation,” *Chemical Physics Letters* **40**, 126–130 (1976).
- ²¹²B. Williams and J. Fleming, “Laser-induced fluorescence detection of acetylene in low-pressure propane and methane flames,” *Applied Physics B* **75**, 883–890 (2002).
- ²¹³G. Inoue and H. Akimoto, “Laser-induced fluorescence of the C₂H₃O radical,” *The Journal of Chemical Physics* **74**, 425–433 (1981).
- ²¹⁴K. Kleinermanns and A. Luntz, “Laser-induced fluorescence of CH₂CHO produced in the crossed molecular beam reactions of O(³P) with Olefins,” *The Journal of Physical Chemistry* **85**, 1966–1968 (1981).
- ²¹⁵L. DiMauro, M. Heaven, and T. A. Miller, “Laser induced fluorescence study of the $\tilde{B}^2A'' \rightarrow \tilde{X}^2A''$ transition of the vinoxy radical in a supersonic free jet expansion,” *The Journal of chemical physics* **81**, 2339–2346 (1984).
- ²¹⁶M. Nakajima, A. Miyoshi, Y. Sumiyoshi, and Y. Endo, “Laser-induced fluorescence and pure rotational spectroscopy of the CH₂CHS (vinylthio) radical,” *The Journal of chemical physics* **126** (2007).
- ²¹⁷G. Inoue, M. Okuda, and H. Akimoto, “Laser-induced fluorescence of the C₂H₅O radical,” *The Journal of Chemical Physics* **75**, 2060–2065 (1981).
- ²¹⁸G. Black and L. E. Jusinski, “Laser-induced fluorescence of C₂H₅S radicals,” *Chemical physics letters* **136**, 241–246 (1987).
- ²¹⁹W.-C. Hung, M.-y. Shen, C.-h. Yu, and Y.-P. Lee, “Vibronic analysis of the $\tilde{B}^2A'' - \tilde{X}^2A''$ laser-induced fluorescence of jet-cooled C₂H₅S,” *The Journal of chemical physics* **105**, 5722–5730 (1996).

- ²²⁰M. Kakimoto and T. Kasuya, "Doppler-limited dye laser excitation spectroscopy of the CCN radical," *Journal of Molecular Spectroscopy* **94**, 380–392 (1982).
- ²²¹K. Hakuta and H. Uehara, "Laser-induced fluorescence spectrum of the CCN radical with an Ar⁺ laser," *The Journal of Chemical Physics* **78**, 6484–6489 (1983).
- ²²²W. Pitts, V. Donnelley, A. Baronavski, and J. McDonald, "C₂O ($\tilde{A}^3\Pi_i \leftrightarrow \tilde{X}^3\Sigma^-$): laser induced excitation and fluorescence spectra," *Chemical Physics* **61**, 451–464 (1981).
- ²²³F. X. Sunahori, J. Wei, and D. J. Clouthier, "The electronic spectrum of the C₂P free radical and a Renner–Teller analysis of the $^2\Delta$ and $\tilde{X}^2\Pi$ electronic states," *The Journal of chemical physics* **128** (2008).
- ²²⁴A. Schoeffler, H. Kohguchi, K. Hoshina, Y. Ohshima, and Y. Endo, "Laser induced fluorescence spectroscopy of the $\tilde{A}_3\Pi_i \leftarrow \tilde{X}^3\Pi^-$ transition of the CCS radical," *The Journal of Chemical Physics* **114**, 6142–6150 (2001).
- ²²⁵T. Ikegami, S. Ishibashi, Y. Yamagata, K. Ebihara, R. Thareja, and J. Narayan, "Spatial distribution of carbon species in laser ablation of graphite target," *Journal of Vacuum Science & Technology A: Vacuum, Surfaces, and Films* **19**, 1304–1307 (2001).
- ²²⁶G. Black and L. E. Jusinski, "Laser-induced fluorescence of i-C₃H₇S radicals," *Chemical physics letters* **139**, 431–436 (1987).
- ²²⁷K. Hoshina and Y. Endo, "Laser induced fluorescence spectroscopy of the C₃N radical," *The Journal of chemical physics* **127** (2007).
- ²²⁸K. Hoshina, H. Kohguchi, Y. Ohshima, and Y. Endo, "Laser-induced fluorescence spectroscopy of the C₄H and C₄D radicals in a supersonic jet," *The Journal of chemical physics* **108**, 3465–3478 (1998).
- ²²⁹B. A. Williams and J. W. Fleming, "Laser-induced fluorescence spectrum of the FCO radical," *The Journal of chemical physics* **106**, 4376–4382 (1997).
- ²³⁰F. X. Sunahori and D. J. Clouthier, "The electronic spectrum of the fluoroborane free radical. II. analysis of laser-induced fluorescence and single vibronic level emission spectra," *The Journal of chemical physics* **130** (2009).
- ²³¹R. Callaghan, Y.-L. Huang, S. Arepalli, and R. J. Gordon, "Single-photon VUV laser-induced fluorescence spectra of HCl and HBr," *Chemical physics letters* **158**, 531–534 (1989).
- ²³²R. König and J. Lademann, "Laser-induced fluorescence detection of HCO produced by laser photolysis of formaldehyde," *Chemical Physics Letters* **94**, 152–155 (1983).
- ²³³G. Inoue and M. Suzuki, "Laser induced fluorescence of HCCO (DCCO) radical formed in O+ C₂H₂ (C₂D₂) reaction," *The Journal of chemical physics* **84**, 3709–3716 (1986).
- ²³⁴M. Nakajima, Y. Yoneda, H. Toyoshima, Y. Sumiyoshi, and Y. Endo, "Gas phase electronic spectrum of the HSCCS radical by laser-induced fluorescence spectroscopy," *Journal of Molecular Spectroscopy* **232**, 255–263 (2005).
- ²³⁵M. Nakajima, Y. Sumiyoshi, and Y. Endo, "Laser induced fluorescence spectroscopy of the HC₄S and DC₄S radicals," *Chemical physics letters* **351**, 359–364 (2002).

- ²³⁶N. Reilly, G. Cupitt, S. Kable, and T. Schmidt, "Experimental and theoretical investigation of the dispersed fluorescence spectroscopy of HC₄S," *The Journal of chemical physics* **124** (2006).
- ²³⁷M. Nakajima, Y. Sumiyoshi, and Y. Endo, "Laser induced fluorescence spectroscopy of the HC₆S radical," *Chemical physics letters* **355**, 116–122 (2002).
- ²³⁸D. R. Crosley, "Laser-induced fluorescence measurement of combustion chemistry intermediates," *High Temperature Materials and Processes* **7**, 41–54 (1986).
- ²³⁹S. Mayama, K. Egashira, and K. Obi, "Laser induced fluorescence of HNO and DNO $\tilde{A}^1A'' - \tilde{X}^1A''$ in a supersonic free jet," *Research on chemical intermediates* **12**, 285–302 (1989).
- ²⁴⁰N. R. Taylor and K. M. Lemmer, "Laser-Induced Fluorescence Detection of Nitroxyl (HNO) Formed from the Thermal Decomposition of Hydroxylammonium Nitrate Vapor," *Journal of Ionic Liquids* , 100084 (2024).
- ²⁴¹H. Harjanto, W. W. Harper, and D. J. Clouthier, "Resolution of anomalies in the geometry and vibrational frequencies of monobromosilylene (HSiBr) by pulsed discharge jet spectroscopy," *The Journal of chemical physics* **105**, 10189–10200 (1996).
- ²⁴²P. Ho, W. G. Breiland, and R. W. Carr, "Kinetics of the reactions of HSiCl with SiH₄ and SiH₂Cl₂," *Chemical physics letters* **132**, 422–426 (1986).
- ²⁴³R. de Nalda, A. Mavromanolakis, S. Couris, and M. Castillejo, "Induced HSiCl emission in the UV photodissociation of 2-chloroethenylsilane," *Chemical Physics Letters* **316**, 449–454 (2000).
- ²⁴⁴W. W. Harper and D. J. Clouthier, "Reinvestigation of the HSiCl electronic spectrum: Experimental reevaluation of the geometry, rotational constants, and vibrational frequencies," *The Journal of chemical physics* **106**, 9461–9473 (1997).
- ²⁴⁵H. U. Lee and J. P. Deneufville, "Laser-induced fluorescence of the HSiF radical," *Chemical physics letters* **99**, 394–398 (1983).
- ²⁴⁶R. Dixon and N. Wright, "The rotational analysis of a Doppler-limited $\tilde{A}^1A'' - \tilde{X}^1A'$ fluorescence excitation spectrum of HSiF at 430 nm," *Chemical physics letters* **117**, 280–285 (1985).
- ²⁴⁷C. J. Evans and M. R. Dover, "Spectroscopic Investigation of the Electronic $\tilde{A}^1A'' - \tilde{X}^1A'$ Transition of HSiNC," *The Journal of Physical Chemistry A* **113**, 8533–8539 (2009).
- ²⁴⁸M. R. Dover, C. J. Evans, and C. M. Western, "Spectroscopic investigation of the $\tilde{A}^1A'' - \tilde{X}^1A'$ electronic transition of HSiNCO," *The Journal of chemical physics* **131** (2009).
- ²⁴⁹Y.-Y. Lee, Y.-P. Lee, and N. S. Wang, "Kinetics of the reaction of HSO with O₃ at temperatures 273–423 K," *The Journal of chemical physics* **100**, 387–392 (1994).
- ²⁵⁰M. Kawasaki, "Laser-induced Fluorescence of Unstable Intermediates in Combustion: HSO and H₂CS," *Laser Diagnostics and Modeling of Combustion* , 203–210 (1987).
- ²⁵¹T. Yoshikawa, A. Watanabe, Y. Sumiyoshi, and Y. Endo, "Laser spectroscopy of the $\tilde{A}A'' - \tilde{X}A''$ system for the HSO radical," *Journal of Molecular Spectroscopy* **254**, 119–125 (2009).

- ²⁵²G. Rothschof, T. C. Smith, and D. J. Clouthier, “Barely fluorescent molecules. I. Twin-discharge jet laser-induced fluorescence spectroscopy of HSnCl and DSnCl,” *The Journal of Chemical Physics* **156** (2022).
- ²⁵³W. Lempert, G. Diskin, V. Kumar, I. Glesk, and R. Miles, “Two-dimensional imaging of molecular hydrogen in H₂-air diffusion flames using two-photon laser-induced fluorescence,” *Optics letters* **16**, 660–662 (1991).
- ²⁵⁴F. Northrup, J. Polanyi, S. Wallace, and J. Williamson, “VUV laser-induced fluorescence of molecular hydrogen,” *Chemical physics letters* **105**, 34–37 (1984).
- ²⁵⁵T. Mosbach, H.-M. Katsch, and H. Döbele, “In situ diagnostics in plasmas of electronic-ground-state hydrogen molecules in high vibrational and rotational states by laser-induced fluorescence with vacuum-ultraviolet radiation,” *Physical Review Letters* **85**, 3420 (2000).
- ²⁵⁶O. Gabriel, D. Schram, and R. Engeln, “Formation and relaxation of rovibrationally excited H₂ molecules due to plasma-surface interaction,” *Physical Review E* **78**, 016407 (2008).
- ²⁵⁷A. A. Turnipseed, M. K. Gilles, J. B. Burkholder, and A. Ravishankara, “LIF detection of IO and the rate coefficients for I+ O₃ and IO+ NO reactions,” *Chemical physics letters* **242**, 427–434 (1995).
- ²⁵⁸W. J. Bloss, T. J. Gravestock, D. E. Heard, T. Ingham, G. P. Johnson, and J. D. Lee, “Application of a compact all solid-state laser system to the in situ detection of atmospheric OH, HO₂, NO and IO by laser-induced fluorescence,” *Journal of Environmental Monitoring* **5**, 21–28 (2003).
- ²⁵⁹B. Hiller and R. Hanson, “Properties of the iodine molecule relevant to laser-induced fluorescence experiments in gas flows,” *Experiments in fluids* **10**, 1–11 (1990).
- ²⁶⁰S. Ezekiel and R. Weiss, “Laser-induced fluorescence in a molecular beam of iodine,” *Physical Review Letters* **20**, 91 (1968).
- ²⁶¹M. Zucco, L. Robertsson, and J. Wallerand, “Laser-induced fluorescence as a tool to verify the reproducibility of iodine-based laser standards: a study of 96 iodine cells,” *Metrologia* **50**, 402 (2013).
- ²⁶²K.-C. Lin and H.-C. Chang, “State-selective reaction of excited potassium atom with hydrogen molecule. K* + H₂ → KH + H,” *The Journal of Chemical Physics* **90**, 6151–6156 (1989).
- ²⁶³W. J. Tango, J. K. Link, and R. N. Zare, “Spectroscopy of K₂ using laser-induced fluorescence,” *The Journal of Chemical Physics* **49**, 4264–4268 (1968).
- ²⁶⁴S. Milosevic, P. Kowalczyk, and G. Pichler, “A study of structured continua in K₂ excited by the 457.9 nm Ar-ion laser line,” *Journal of Physics B: Atomic and Molecular Physics* **20**, 2231 (1987).
- ²⁶⁵K. Meiwes and F. Engelke, “Predissociation of K₂: molecular beam-laser-induced fluorescence spectroscopy of the C¹Π_u – X¹Σ_g⁺ band system,” *Chemical Physics Letters* **85**, 409–414 (1982).
- ²⁶⁶A. Ross, C. Effantin, J. d’Incan, and R. Barrow, “Laser-induced fluorescence of NaK: the b(1) ³Π state,” *Journal of Physics B: Atomic and Molecular Physics* **19**, 1449 (1986).
- ²⁶⁷W. Demtröder, M. McClintock, and R. Zare, “Spectroscopy of Na₂ using laser-induced fluorescence,” *The Journal of Chemical Physics* **51**, 5495–5508 (1969).

- ²⁶⁸R. A. Copeland, D. R. Crosley, and G. P. Smith, "Laser-induced fluorescence spectroscopy of NCO and NH₂ in atmospheric pressure flames," Symposium (International) on Combustion **20**, 1195–1203 (1985).
- ²⁶⁹T. Yoshikawa, Y. Sumiyoshi, H. Takada, K. Hoshina, and Y. Endo, "Laser induced fluorescence spectroscopy of NC₃O," The Journal of chemical physics **128** (2008).
- ²⁷⁰M. Nakajima, Y. Yoneda, Y. Sumiyoshi, and Y. Endo, "Laser-induced fluorescence spectroscopy of NC₃S," The Journal of chemical physics **120**, 2662–2666 (2004).
- ²⁷¹R. Heidner III, H. Helvajian, J. Holloway, and J. B. Koffend, "Direct observation of NF(X) using laser-induced fluorescence: kinetics of the NF ³Σ⁻ ground state," The Journal of Physical Chemistry **93**, 7813–7818 (1989).
- ²⁷²G. Wang, S. Wang, and T. F. Guiberti, "Simultaneous planar laser-induced fluorescence measurement of reactant NH₃, radical NH, and pollutant NO in ammonia-hydrogen flames using a single dye laser," Combustion and Flame **256**, 112981 (2023).
- ²⁷³R. A. Copeland, M. L. Wise, K. J. Rensberger, and D. R. Crosley, "Time resolved laser induced fluorescence of the NH radical in low pressure N₂O flames," Applied optics **28**, 3199–3205 (1989).
- ²⁷⁴H. Umemoto and K.-i. Matsumoto, "Production of NH (ND) Radicals in the Reactions of N (²D) with H₂ (D₂): Nascent Vibrational Distributions of NH (X ³Σ⁻) and ND (X³Σ⁻)," The Journal of chemical physics **104**, 9640–9643 (1996).
- ²⁷⁵J. Halpern, G. Hancock, M. Lenzi, and K. Welge, "Laser induced fluorescence from NH₂(²A₁). State selected radiative lifetimes and collisional de-excitation rates," The Journal of Chemical Physics **63**, 4808–4816 (1975).
- ²⁷⁶G. Hancock, W. Lange, M. Lenzi, and K. Welge, "Laser fluorescence of NH₂ and rate constant measurement of NH₂+ NO," Chemical Physics Letters **33**, 168–172 (1975).
- ²⁷⁷U. Westblom and M. Alden, "Laser-induced fluorescence detection of NH₃ in flames with the use of two-photon excitation," Applied spectroscopy **44**, 881–886 (1990).
- ²⁷⁸R. Beaman, T. Nelson, D. Richards, and D. Setser, "Observation of azido radical by laser-induced fluorescence," Journal of Physical Chemistry **91**, 6090–6092 (1987).
- ²⁷⁹C. Brackmann, J. Bood, J. D. Naucler, A. A. Konnov, and M. Alden, "Quantitative picosecond laser-induced fluorescence measurements of nitric oxide in flames," Proceedings of the Combustion Institute **36**, 4533–4540 (2017).
- ²⁸⁰A. Van Gessel, B. Hrycak, M. Jasiński, J. Mizeraczyk, J. Van Der Mullen, and P. Bruggeman, "Temperature and NO density measurements by LIF and OES on an atmospheric pressure plasma jet," Journal of Physics D: Applied Physics **46**, 095201 (2013).
- ²⁸¹M. P. Lee, B. K. McMillin, and R. K. Hanson, "Temperature measurements in gases by use of planar laser-induced fluorescence imaging of NO," Applied Optics **32**, 5379–5396 (1993).
- ²⁸²A. Wodtke, L. Huwel, H. Schluter, G. Meijer, P. Andersen, and H. Voges, "High-sensitivity detection of NO in a flame using a tunable ArF laser," Optics letters **13**, 910–912 (1988).

- ²⁸³A. Delon and R. Jost, “Laser induced dispersed fluorescence spectra of jet cooled NO₂: The complete set of vibrational levels up to 10 000 cm⁻¹ and the onset of the $\tilde{X}^2A_1 - \tilde{A}^2B_2$ vibronic interaction,” *The Journal of chemical physics* **95**, 5686–5700 (1991).
- ²⁸⁴B. Kim, P. L. Hunter, and H. Johnston, “NO₃ radical studied by laser-induced fluorescence,” *The Journal of chemical physics* **96**, 4057–4067 (1992).
- ²⁸⁵M. Fukushima, “Laser induced fluorescence spectra of the $\tilde{B}^2E' - \tilde{X}^2A_2'$ transition of jet cooled ¹⁴NO₃ and ¹⁵NO₃ I: ν_4 progressions in the ground \tilde{X}^2A_2' state,” *Journal of Molecular Spectroscopy* **387**, 111646 (2022).
- ²⁸⁶J. B. Jeffries and D. R. Crosley, “Laser-induced fluorescence detection of the NS radical in sulfur and nitrogen doped methane flames,” *Combustion and flame* **64**, 55–64 (1986).
- ²⁸⁷A. P. Ongstad, R. I. Lawconnell, and T. L. Henshaw, “Photodissociation dynamics of S₄N₄ at 222 and 248 nm,” *The Journal of chemical physics* **97**, 1053–1064 (1992).
- ²⁸⁸J. Goldsmith and R. Anderson, “Laser-induced fluorescence spectroscopy and imaging of molecular oxygen in flames,” *Optics letters* **11**, 67–69 (1986).
- ²⁸⁹A. M. Irvine, I. W. Smith, R. P. Tuckett, and X.-F. Yang, “A laser-induced fluorescence determination of the complete internal state distribution of OH produced in the reaction: H+ NO₂ → OH+ NO,” *The Journal of chemical physics* **93**, 3177–3186 (1990).
- ²⁹⁰C. Zhu, H. Wang, B. Chen, Y. Chen, T. Yang, J. Yin, and J. Liu, “Fine and hyperfine interactions of PbF studied by laser-induced fluorescence spectroscopy,” *The Journal of chemical physics* **157** (2022).
- ²⁹¹B. Chen, Y.-N. Chen, J.-N. Pan, J.-P. Yin, and H.-L. Wang, “Spectroscopic study of B²Σ⁺ – X²Π_{1/2} transition of electron electric dipole moment candidate PbF,” *Chinese Physics B* **31**, 093301 (2022).
- ²⁹²O. Shestakov, A. Pravilov, H. Demes, and E. Fink, “Radiative lifetime and quenching of the A²Σ⁺ and X²Π_{3/2} states of PbF,” *Chemical physics* **165**, 415–427 (1992).
- ²⁹³Y. Chen, Q. Zhang, D. Zhang, C. Chen, S. Yu, and X. Ma, “Laser-induced fluorescence spectrum of PH₂ cooled in a supersonic jet,” *Chemical physics letters* **223**, 104–109 (1994).
- ²⁹⁴R. E. Huie, N. J. Long, and B. A. Thrush, “Laser induced fluorescence of the PH₂ radical,” *Journal of the Chemical Society, Faraday Transactions 2: Molecular and Chemical Physics* **74**, 1253–1262 (1978).
- ²⁹⁵C. N. Xuan and A. Margani, “Dynamics and spectroscopy of PH₂ (\tilde{A}^2A_1),” *The Journal of chemical physics* **93**, 136–146 (1990).
- ²⁹⁶M. A. Clyne and M. C. Heaven, “Laser-induced fluorescence of the PO radical,” *Chemical Physics* **58**, 145–150 (1981).
- ²⁹⁷K. N. Wong, W. R. Anderson, and A. J. Kotlar, “Radiative processes following laser excitation of the A²Σ⁺ state of PO,” *The Journal of chemical physics* **85**, 2406–2413 (1986).
- ²⁹⁸N. Wang, Y. Ng, and A.-C. Cheung, “Laser induced fluorescence spectroscopy of ruthenium monoboride,” *Chemical Physics Letters* **547**, 21–23 (2012).

- ²⁹⁹R. S. DaBell, R. G. Meyer, and M. D. Morse, “Electronic structure of the 4d transition metal carbides: Dispersed fluorescence spectroscopy of MoC, RuC, and PdC,” *The Journal of Chemical Physics* **114**, 2938–2954 (2001).
- ³⁰⁰H. Zarringhalam, *High-resolution laser and far-infrared Fourier transform synchrotron-based spectroscopy of selected molecules*, Ph.D. thesis, University of New Brunswick (2022).
- ³⁰¹T. C. Steimle and W. Virgo, “The permanent electric dipole moments and magnetic hyperfine interactions of ruthenium mononitride, RuN,” *The Journal of chemical physics* **119**, 12965–12972 (2003).
- ³⁰²J. Tsee, F. Wampler, R. Oldenborg, and W. Rice, “Spectroscopy and reaction kinetics of HS radicals,” *Chemical physics letters* **82**, 80–84 (1981).
- ³⁰³W. Hawkins and P. Houston, “193 nm photodissociation of H₂S: The SH internal energy distribution,” *The Journal of Chemical Physics* **73**, 297–302 (1980).
- ³⁰⁴K. Becker, D. HAAKS, and T. TATARCZYK, “Lifetime measurements at selectively excited-states of diatomic hydrides,” *Berichte Der Bunsen-Gesellschaft-Physical Chemistry Chemical Physics* **78**, 1157–1160 (1974).
- ³⁰⁵I. P. Herman, V. M. Donnelly, C.-C. Cheng, and K. V. Guinn, “Surface analysis during plasma etching by laser-induced thermal desorption,” *Japanese journal of applied physics* **35**, 2410 (1996).
- ³⁰⁶C. Cheng, K. Guinn, I. Herman, and V. Donnelly, “Competitive halogenation of silicon surfaces in HBr/Cl₂ plasmas studied with x-ray photoelectron spectroscopy and in situ, real-time, pulsed laser-induced thermal desorption,” *Journal of Vacuum Science & Technology A: Vacuum, Surfaces, and Films* **13**, 1970–1976 (1995).
- ³⁰⁷G. Rothschof, T. C. Smith, and D. J. Clouthier, “The high-resolution LIF spectrum of the SiCCl free radical: Probing the silicon-carbon triple bond,” *Journal of Molecular Spectroscopy* **359**, 22–30 (2019).
- ³⁰⁸G. Rothschof, T. C. Smith, and D. J. Clouthier, “Laser-induced fluorescence detection of the elusive SiCF free radical,” *The Journal of Chemical Physics* **149** (2018).
- ³⁰⁹T. C. Smith, H. Li, D. J. Clouthier, C. T. Kingston, and A. J. Merer, “The electronic spectrum of silicon methyldiyne (SiCH), a molecule with a silicon-carbon triple bond in the excited state,” *The Journal of Chemical Physics* **112**, 3662–3670 (2000).
- ³¹⁰S. Singleton, K. G. McKendrick, R. A. Copeland, and J. B. Jeffries, “Vibrational transition probabilities in the B–X and B’–X systems of the chlorosilyldiyne radical,” *The Journal of Physical Chemistry* **96**, 9703–9709 (1992).
- ³¹¹M. Suzuki, N. Washida, and G. Inoue, “Laser-induced fluorescence of the SiCl₂ radical,” *Chemical Physics Letters* **131**, 24–30 (1986).
- ³¹²T. C. Smith and D. J. Clouthier, “Identification of the Jahn–Teller active trichlorosiloxy (SiCl₃O) free radical in the gas phase,” *The Journal of Chemical Physics* **152** (2020).
- ³¹³H. Umeki, M. Nakajima, and Y. Endo, “Laser spectroscopy of the $\tilde{A}^2\Sigma^+ - \tilde{X}^2\Pi_i$ band system of l-SiC₃H,” *The Journal of Chemical Physics* **143** (2015).

- ³¹⁴G. Hebner, “Spatially resolved SiF and SiF₂ densities in inductively driven discharges containing C₂F₆ and C₄F₈,” *Journal of Applied Physics* **90**, 4938–4945 (2001).
- ³¹⁵Y. Nozaki, K. Kongo, T. Miyazaki, M. Kitazoe, K. Horii, H. Umemoto, A. Masuda, and H. Matsumura, “Identification of Si and SiH in catalytic chemical vapor deposition of SiH₄ by laser induced fluorescence spectroscopy,” *Journal of Applied Physics* **88**, 5437–5443 (2000).
- ³¹⁶M. Hertl, N. Dorval, O. Leroy, J. Jolly, and M. Péalat, “Laser-induced fluorescence measurements of absolute SiH densities in-RF discharges and comparison with a numerical model,” *Plasma Sources Science and Technology* **7**, 130 (1998).
- ³¹⁷Y. Matsumi, T. Hayashi, H. Yoshikawa, and S. Komiya, “Laser diagnostics of a silane plasma—SiH radicals in an a-Si: H chemical vapor deposition system,” *Journal of Vacuum Science & Technology A: Vacuum, Surfaces, and Films* **4**, 1786–1790 (1986).
- ³¹⁸M. Hertl and J. Jolly, “Laser-induced fluorescence detection and kinetics of SiH₂ radicals in Ar/H₂/SiH₄ RF discharges,” *Journal of Physics D: Applied Physics* **33**, 381 (2000).
- ³¹⁹A. Kono, N. Koike, K. Okuda, and T. G. T. Goto, “Laser-induced-fluorescence detection of SiH₂ radicals in a radio-frequency silane plasma,” *Japanese journal of applied physics* **32**, L543 (1993).
- ³²⁰A. Kono, N. Koike, H. Nomura, and T. G. T. Goto, “Laser-induced-fluorescence study of the SiH₂ density in RF SiH₄ plasmas with Xe, Ar, He, and H₂ dilution gases,” *Japanese journal of applied physics* **34**, 307 (1995).
- ³²¹R. Walkup, P. Avouris, R. Dreyfus, J. Jasinski, and G. Selwyn, “Laser detection of diatomic products of plasma sputtering and etching,” *Applied physics letters* **45**, 372–374 (1984).
- ³²²R. S. Chrystie, O. M. Feroughi, T. Dreier, and C. Schulz, “SiO multi-line laser-induced fluorescence for quantitative temperature imaging in flame-synthesis of nanoparticles,” *Applied Physics B* **123**, 1–12 (2017).
- ³²³R. S. Chrystie, F. L. Ebertz, T. Dreier, and C. Schulz, “Absolute SiO concentration imaging in low-pressure nanoparticle-synthesis flames via laser-induced fluorescence,” *Applied Physics B* **125**, 1–15 (2019).
- ³²⁴K. Greenberg and P. Hargis Jr, “Laser-induced-fluorescence detection of SO and SO₂ in SF₆/O₂ plasma-etching discharges,” *Journal of applied physics* **68**, 505–511 (1990).
- ³²⁵W. Weng, M. Aldeén, and Z. Li, “Quantitative SO₂ detection in combustion environments using broad band ultraviolet absorption and laser-induced fluorescence,” *Analytical chemistry* **91**, 10849–10855 (2019).
- ³²⁶A. L. Smith and J. B. Hopkins, “Fluorescence of S₂(B–X) excited by fixed frequency ultraviolet lasers,” *The Journal of Chemical Physics* **75**, 2080–2084 (1981).
- ³²⁷Q. Zhang, P. Dupré, B. Grzybowski, and P. H. Vaccaro, “Laser-induced fluorescence studies of jet-cooled S₂O: Axis-switching and predissociation effects,” *The Journal of chemical physics* **103**, 67–79 (1995).
- ³²⁸S. Nakhate, S. Mukund, and S. Bhattacharyya, “Jet cooled laser-induced fluorescence spectroscopy of tantalum monocarbide: Observation of the ground state vibrations and the low-energy states,” *Journal of Molecular Structure* **1243**, 130888 (2021).

- ³²⁹S. Nakhate, S. Mukund, and S. Bhattacharyya, “Laser-induced fluorescence spectroscopy of jet-cooled TiC: Observation of low-lying $^1\Sigma^+$ states,” *Chemical Physics Letters* **680**, 51–55 (2017).
- ³³⁰Z. Zhang, J. Guo, X. Yu, J. Zhen, and Y. Chen, “The laser-induced fluorescence spectroscopy of TiF in the ultraviolet region,” *Journal of Molecular Spectroscopy* **253**, 112–115 (2009).
- ³³¹N. Zhao, D. Lei, X. Li, J. Li, Q. Ma, Q. Zhang, L. Guo, and Y. Lu, “Experimental investigation of laser-induced breakdown spectroscopy assisted with laser-induced fluorescence for trace aluminum detection in steatite ceramics,” *Applied optics* **58**, 1895–1899 (2019).
- ³³²R. Dreyfus, R. Kelly, and R. Walkup, “Laser-induced fluorescence studies of excimer laser ablation of Al_2O_3 ,” *Applied physics letters* **49**, 1478–1480 (1986).
- ³³³G. S. Selwyn, “Atomic arsenic detection by ArF laser-induced fluorescence,” *Applied physics letters* **51**, 167–168 (1987).
- ³³⁴C. Li, Z. Hao, Z. Zou, R. Zhou, J. Li, L. Guo, X. Li, Y. Lu, and X. Zeng, “Determinations of trace boron in superalloys and steels using laser-induced breakdown spectroscopy assisted with laser-induced fluorescence,” *Optics Express* **24**, 7850–7857 (2016).
- ³³⁵X. Aubert, C. Duluard, N. Sadeghi, and A. Gicquel, “Comparison of three optical diagnostic techniques for the measurement of boron atom density in a $\text{H}_2/\text{B}_2\text{H}_6$ microwave plasma,” *Plasma Sources Science and Technology* **26**, 115011 (2017).
- ³³⁶N. Sirse, M. Foucher, P. Chabert, and J.-P. Booth, “Ground state bromine atom density measurements by two-photon absorption laser-induced fluorescence,” *Plasma Sources Science and Technology* **23**, 062003 (2014).
- ³³⁷M. Aldén, P.-E. Bengtsson, and U. Westblom, “Detection of carbon atoms in flames using stimulated emission induced by two-photon laser excitation,” *Optics Communications* **71**, 263–268 (1989).
- ³³⁸J. Booth, Y. Azamoum, N. Sirse, and P. Chabert, “Absolute atomic chlorine densities in a Cl_2 inductively coupled plasma determined by two-photon laser-induced fluorescence with a new calibration method,” *Journal of Physics D: Applied Physics* **45**, 195201 (2012).
- ³³⁹M. Heaven, T. A. Miller, R. R. Freeman, J. White, and J. Bokor, “Two-photon absorption, laser-induced fluorescence detection of Cl atoms,” *Chemical Physics Letters* **86**, 458–462 (1982).
- ³⁴⁰W. Sdorra, A. Quentmeier, and K. Niemax, “Basic investigations for laser microanalysis: II. Laser-induced fluorescence in laser-produced sample plumes,” *Microchimica Acta* **98**, 201–218 (1989).
- ³⁴¹B. Gellert, “Measurement of high copper vapour densities by laser-induced fluorescence,” *Journal of Physics D: Applied Physics* **21**, 710 (1988).
- ³⁴²M. Bolshov, A. Zybin, and I. Smirenkina, “Atomic fluorescence spectrometry with laser excitation,” *Spectrochimica Acta Part B: Atomic Spectroscopy* **36**, 1143–1152 (1981).
- ³⁴³H. Falk, H.-J. Paetzold, K. Schmidt, and J. Tilch, “Analytical application of laser excited atomic fluorescence using a graphite cup atomizer,” *Spectrochimica Acta Part B: Atomic Spectroscopy* **43**, 1101–1109 (1988).

- ³⁴⁴W. MA, S. TAO, D. ZHANG, and D. CHEN, “Determination of trace gallium in rock and sediment samples by laser-induced fluorescence spectrometry,” *Analytical Sciences/Supplements* **17**, a215–a218 (2002).
- ³⁴⁵P. Brewer, P. Das, G. Ondrey, and R. Bersohn, “Measurement of the relative populations of I ($^2P_{1/2}^0$) and I ($^2P_{3/2}^0$) by laser induced vacuum ultraviolet fluorescence,” *The Journal of Chemical Physics* **79**, 720–723 (1983).
- ³⁴⁶K. Zhu, S. J. Barkley, C. E. Dedic, T. R. Sippel, and J. B. Michael, “Two-photon laser-induced fluorescence of sodium in multiphase combustion,” *Applied Optics* **59**, 5632–5641 (2020).
- ³⁴⁷J. W. Daily and C. Chan, “Laser-induced fluorescence measurement of sodium in flames,” *Combustion and Flame* **33**, 47–53 (1978).
- ³⁴⁸T. Erdmann, H. Figger, and H. Walther, “Lifetime measurements with a tunable flashlamp pumped dye laser,” *Optics Communications* **6**, 166–168 (1972).
- ³⁴⁹S. Laville, C. Goueguel, H. Loudyi, F. Vidal, M. Chaker, and M. Sabsabi, “Laser-induced fluorescence detection of lead atoms in a laser-induced plasma: An experimental analytical optimization study,” *Spectrochimica Acta Part B: Atomic Spectroscopy* **64**, 347–353 (2009).
- ³⁵⁰P. Brewer, N. Van Veen, and R. Bersohn, “Two-photon induced fluorescence and resonance-enhanced ionization of sulfur atoms,” *Chemical Physics Letters* **91**, 126–129 (1982).
- ³⁵¹R. Roth, K. Spears, and G. Wong, “Spatial concentrations of silicon atoms by laser-induced fluorescence in a silane glow discharge,” *Applied physics letters* **45**, 28–30 (1984).
- ³⁵²N. Britun, M. Gaillard, and J. Han, “Laser induced fluorescence for Ti and Ti⁺ density characterization in a magnetron discharge,” *Journal of Physics D: Applied Physics* **41**, 185201 (2008).
- ³⁵³P. Ljung, E. Nyström, J. Enger, P. Ljungberg, and O. Axner, “Detection of titanium in electrothermal atomizers by laser-induced fluorescence. Part 1. Determination of optimum excitation and detection wavelengths,” *Spectrochimica Acta Part B: Atomic Spectroscopy* **52**, 675–701 (1997).
- ³⁵⁴S. Hadrath, J. Ehlbeck, G. Lieder, and F. Sigeneger, “Determination of absolute population densities of eroded tungsten in hollow cathode lamps and fluorescent lamps by laser-induced fluorescence,” *Journal of Physics D: Applied Physics* **38**, 3285 (2005).
- ³⁵⁵A. Georgiev, A. Blagoev, and A. Pashov, “Detection of neutral tungsten by laser-induced fluorescence,” *AIP Conference Proceedings* **2075** (2019).
- ³⁵⁶T. Lunt, G. Fussmann, and O. Waldmann, “Experimental investigation of the plasma-wall transition,” *Physical review letters* **100**, 175004 (2008).
- ³⁵⁷Y. Tanida, D. Kuwahara, and S. Shinohara, “Spatial profile of ion velocity distribution function in helicon high-density plasma by laser induced fluorescence method,” *Transactions of the Japan Society for Aeronautical and Space Sciences, Aerospace Technology Japan* **14**, Pb_7–Pb_12 (2016).

- ³⁵⁸S. C. Thakur, J. Gosselin, J. McKee, E. Scime, S. Sears, and G. Tynan, “Development of core ion temperature gradients and edge sheared flows in a helicon plasma device investigated by laser induced fluorescence measurements,” *Physics of Plasmas* **23** (2016).
- ³⁵⁹C. Biloiu, X. Sun, E. Choueiri, F. Doss, E. Scime, J. Heard, R. Spektor, and D. Ventura, “Evolution of the parallel and perpendicular ion velocity distribution functions in pulsed helicon plasma sources obtained by time resolved laser induced fluorescence,” *Plasma Sources Science and Technology* **14**, 766 (2005).
- ³⁶⁰G. Severn, X. Wang, E. Ko, N. Hershkowitz, M. Turner, and R. McWilliams, “Ion flow and sheath physics studies in multiple ion species plasmas using diode laser based laser-induced fluorescence,” *Thin Solid Films* **506**, 674–678 (2006).
- ³⁶¹T. Bieber, S. Bardin, L. De Poucques, F. Brochard, R. Hugon, J. Vasseur, and J. Bougdira, “Measurements on argon ion by tunable diode-laser induced fluorescence in a low magnetic field helicon configuration reactor,” *Plasma Sources Science and Technology* **20**, 015023 (2011).
- ³⁶²A. M. Keesee, E. E. Scime, and R. F. Boivin, “Laser-induced fluorescence measurements of three plasma species with a tunable diode laser,” *Review of Scientific Instruments* **75**, 4091–4093 (2004).
- ³⁶³D. Kuwahara, Y. Tanida, M. Watanabe, N. Teshigahara, Y. Yamagata, and S. Shinohara, “Development of Ar I and Ar II measuring system using laser-induced fluorescence methods in high-density helicon plasma,” *Plasma and Fusion Research* **10**, 3401057–3401057 (2015).
- ³⁶⁴G. Severn, D. Edrich, and R. McWilliams, “Argon ion laser-induced fluorescence with diode lasers,” *Review of Scientific Instruments* **69**, 10–15 (1998).
- ³⁶⁵T. Harris, J. Eland, and R. Tuckett, “The AX system of Br_2^+ radical cations,” *Journal of Molecular Spectroscopy* **98**, 269–281 (1983).
- ³⁶⁶S. K. S. Kumagai, M. S. M. Sasaki, M. K. M. Koyanagi, and K. H. K. Hane, “Detection of metastable chlorine ions in time-modulated plasma by time resolved laser-induced fluorescence,” *Japanese Journal of Applied Physics* **38**, 7126 (1999).
- ³⁶⁷M. Malyshev, N. Fuller, K. Bogart, V. Donnelly, and I. P. Herman, “Laser-induced fluorescence and langmuir probe determination of Cl_2^+ and Cl^+ absolute densities in transformer-coupled chlorine plasmas,” *Applied physics letters* **74**, 1666–1668 (1999).
- ³⁶⁸V. Bondybey, J. English, and T. A. Miller, “Laser induced fluorescence spectrum of matrix isolated CS_2^+ ,” *The Journal of Chemical Physics* **70**, 1621–1625 (1979).
- ³⁶⁹C.-C. Zen and Y.-P. Lee, “Laser-induced fluorescence of the $\text{A}^2\Pi_u - \text{X}^2\Pi_g$ transition of CS_2^+ in solid Ne. Reanalysis of vibronic spectra,” *Chemical physics letters* **244**, 177–182 (1995).
- ³⁷⁰M. Nakajima, Y. Yoneda, Y. Sumiyoshi, T. Nagata, and Y. Endo, “Laser-induced fluorescence and fluorescence depletion spectroscopy of SCCS^- ,” *The Journal of chemical physics* **119**, 7805–7813 (2003).
- ³⁷¹T. E. Steinberger and E. E. Scime, “Laser-induced fluorescence of singly ionized iodine,” *Journal of Propulsion and Power* **34**, 1235–1239 (2018).

- ³⁷²A. Lejeune, G. Bourgeois, and S. Mazouffre, “Kr II and Xe II axial velocity distribution functions in a cross-field ion source,” *Physics of Plasmas* **19** (2012).
- ³⁷³W. Hargus, G. M. Azarnia, and M. R. Nakles, “Demonstration of laser-induced fluorescence on a krypton hall effect thruster,” in *32nd International Electric Propulsion Conference* (2011) pp. 11–15.
- ³⁷⁴M. Tremblay, B. W. Smith, and J. D. Winefordner, “Laser-excited ionic fluorescence spectrometry of rare-earth elements in the inductively-coupled plasma,” *Analytica chimica acta* **199**, 111–118 (1987).
- ³⁷⁵B. Woodcock, J. Busby, T. Freearge, and G. Hancock, “Doppler spectroscopic measurements of sheath ion velocities in radio-frequency plasmas,” *Journal of applied physics* **81**, 5945–5949 (1997).
- ³⁷⁶M. A. Gharaibeh and D. J. Clouthier, “A laser-induced fluorescence study of the jet-cooled nitrous oxide cation (N_2O^+),” *The Journal of Chemical Physics* **136** (2012).
- ³⁷⁷J. Li, V. M. Bierbaum, and S. R. Leone, “Laser-induced fluorescence study of two weak vibrational bands of the O_2^+ $\text{A}^2\Pi_u\text{-X}^2\Pi_g$ system,” *Chemical Physics Letters* **330**, 331–338 (2000).
- ³⁷⁸Y. Matsuo, T. Nakajima, T. Kobayashi, and M. Takami, “Formation and laser-induced-fluorescence study of SiO^+ ions produced by laser ablation of Si in oxygen gas,” *Applied physics letters* **71**, 996–998 (1997).
- ³⁷⁹T. Smith, B. Ngom, J. Linnell, and A. Gallimore, “Diode laser-induced fluorescence of xenon ion velocity distributions,” in *41st AIAA/ASME/SAE/ASEE Joint Propulsion Conference & Exhibit* (2005) p. 4406.
- ³⁸⁰T. Smith, D. Herman, A. Gallimore, and G. Williams, “Laser-induced fluorescence velocimetry of Xe II in the 30-cm NSTAR-type ion engine plume,” in *40th AIAA/ASME/SAE/ASEE Joint Propulsion Conference and Exhibit* (2004) p. 3963.
- ³⁸¹N. Sadeghi, M. Van De Grift, D. Vender, G. Kroesen, and F. De Hoog, “Transport of argon ions in an inductively coupled high-density plasma reactor,” *Applied physics letters* **70**, 835–837 (1997).
- ³⁸²R. Engeln, S. Mazouffre, P. Vankan, D. Schram, and N. Sadeghi, “Flow dynamics and invasion by background gas of a supersonically expanding thermal plasma,” *Plasma Sources Science and Technology* **10**, 595 (2001).
- ³⁸³Z. D. Short, M. U. Siddiqui, M. F. Henriquez, J. S. McKee, and E. E. Scime, “A novel laser-induced fluorescence scheme for Ar-I in a plasma,” *Review of Scientific Instruments* **87** (2016).
- ³⁸⁴R. Bergert, L. W. Isberner, S. Mitic, and M. H. Thoma, “Quantitative evaluation of laser-induced fluorescence in magnetized low-pressure argon plasma,” *Physics of Plasmas* **28** (2021).
- ³⁸⁵S. Hansen, G. Luckman, G. C. Nieman, and S. D. Colson, “Formation and decay of metastable fluorine atoms in pulsed fluorocarbon/oxygen discharges monitored by laser-induced fluorescence,” *Applied physics letters* **56**, 719–721 (1990).
- ³⁸⁶M. J. Frost, S. Himmelmann, and D. Palmer, “Laser-induced fluorescence studies of elementary processes in a helium plasma following He $3^3\text{P}\text{-}2^3\text{S}$ and $3^1\text{P}\text{-}2^1\text{S}$ excitation,” *Journal of Physics B: Atomic, Molecular and Optical Physics* **34**, 1569 (2001).

- ³⁸⁷W. Rellergert, S. Cahn, A. Garvan, J. Hanson, W. Lippincott, J. Nikkel, and D. McKinsey, "Detection and imaging of He₂ molecules in superfluid helium," *Physical review letters* **100**, 025301 (2008).
- ³⁸⁸W. Hargus, "A preliminary study of krypton laser-induced fluorescence," in *46th AIAA/ASME/SAE/ASEE Joint Propulsion Conference & Exhibit* (2010) p. 6524.
- ³⁸⁹M. Mustafa, M. B. Hunt, N. J. Parziale, M. S. Smith, and E. C. Marineau, "Krypton tagging velocimetry (KTV) investigation of shock-wave/turbulent boundary-layer interaction," in *55th AIAA Aerospace Sciences Meeting* (2017) p. 0025.
- ³⁹⁰S. Nemschokmichal, F. Bernhardt, B. Krames, and J. Meichsner, "Laser-induced fluorescence spectroscopy of N₂(A³Σ_u⁺) and absolute density calibration by Rayleigh scattering in capacitively coupled RF discharges," *Journal of Physics D: Applied Physics* **44**, 205201 (2011).
- ³⁹¹R. Ono, C. Tobaru, Y. Teramoto, and T. Oda, "Laser-induced fluorescence of N₂(A³Σ_u⁺) metastable in N₂ pulsed positive corona discharge," *Plasma Sources Science and Technology* **18**, 025006 (2009).
- ³⁹²X. Shen, H. Wang, Z. Xie, Y. Gao, H. Ling, and Y. Lu, "Detection of trace phosphorus in steel using laser-induced breakdown spectroscopy combined with laser-induced fluorescence," *Applied optics* **48**, 2551–2558 (2009).
- ³⁹³H. Kondo, N. Hamada, and K. Wagatsuma, "Determination of phosphorus in steel by the combined technique of laser induced breakdown spectrometry with laser induced fluorescence spectrometry," *Spectrochimica Acta Part B: Atomic Spectroscopy* **64**, 884–890 (2009).
- ³⁹⁴S. Mazouffre, G. Bourgeois, L. Garrigues, and E. Pawelec, "A comprehensive study on the atom flow in the cross-field discharge of a hall thruster," *Journal of Physics D: Applied Physics* **44**, 105203 (2011).
- ³⁹⁵R. Cedolin, W. Hargus Jr, P. Storm, R. Hanson, and M. Cappelli, "Laser-induced fluorescence study of a xenon hall thruster," *Applied Physics B* **65**, 459–469 (1997).